IEEE Access
Multidisciplinary | Rapid Review | Open Access Journal

Received 21 December 2022, accepted 10 January 2023, date of publication 16 January 2023, date of current version 19 January 2023.

Digital Object Identifier 10.1109/ACCESS.2023.3237214

RESEARCH ARTICLE

The Loss and Efficiency Analysis and Research of Interior Permanent Magnet Synchronous Motors for Traction Applications

LIANBO NIU[1,2] AND MINGZHU ZHANG[1]

[1]School of Mechanical and Electronically Engineering, Henan University of Science and Technology, Luoyang 471003, China
[2]School of Mechanical and Electronically Engineering, Xinxiang University, Xinxiang 453003, China

Corresponding author: Lianbo Niu (niulianbo@163.com)

ABSTRACT An IPMSM with I2V type rotor topology structure is proposed, its loss, efficiency and torque are analyzed and compared with V and IV type. Firstly, the optimized rotor topology structures are used to analyze the no-load air-gap flux density waveform and harmonic contents of the IPMSM. The results show that the THD of the no-load air-gap flux density with the I2V type is the smallest and the sinusoidal degree of the waveform is the highest. Secondly, the loss of the IPMSM with optimized rotor topology structures are analyzed and compared. Compared with the other two rotors, the results show that the iron loss of the IPMSM with the I2V type is the smallest. The iron loss of the IPMSM with I2V type is significantly less than that of the other two rotors especially under the deep flux weakening conditions. The output torque of the IPMSM under different current angles, current densities and speed are analyzed and compared. The results show that the torque performance of the IPMSM with I2V type is better than the other two rotors. this paper proposes a simple and effective method to optimize the position and diameter of the magnetic isolation holes by establishing a parameterized model. The results show that the torque ripple and cogging torque with the further optimized I2V type rotor topology structure are greatly reduced, the iron loss and magnet loss are also effectively reduced. Finally, the von Mises stress and the total displacement of the rotor deformation of the IPMSM with the further optimized I2V type under different working conditions are verified by finite element analysis. The results show that the rotor will not rupture, the displacement is small enough to avoid the touch between stator and rotor.

INDEX TERMS Interior permanent magnet synchronous motor (IPMSM), torque, iron loss, efficiency, magnetic isolation hole.

I. INTRODUCTION

With the global energy crisis and environmental pollution becoming increasingly prominent, energy saving and green electric vehicle (EV) have received more and more attention. As the driving motor is the core technology of the EV, the requirements for relevant technologies of the motor for the EV application are constantly increasing, and the motor for EV application is gradually developing in the direction of high power density, high efficiency, constant power wide speed range and energy saving [1]. Compared with the surface mounted permanent magnet synchronous motor, the IPMSM has higher mechanical strength, high power density, smaller volume and lighter mass, so it has attracted more and more attention from domestic and foreign scholars [2]. Improving torque density and rated speed is an effective method to design the IPMSM with high power density, at this time the current density and the heat load have reached maximum limit that the material of the motor can bear. The greater the unit volume loss of the motor, the more serious the heating phenomenon and the higher the temperature rise, which not only can affect the performance of the IPMSM, such as torque density and efficiency, and cause the decline of the permanent magnet performance and even cause the risk of irreversible demagnetization of the permanent magnet, but also may put forward higher requirements on the insulation

The associate editor coordinating the review of this manuscript and approving it for publication was Zhong Wu.

level of the winding. Therefore, it is very important to have the precise calculation of the losses of the IPMSM, collaborative optimization of electromagnetic and thermal design, avoid the temperature distribution in the IPMSM exceeding the maximum temperature required by the permanent magnet and winding insulation. Under the premise of ensuring the safe and reliable operation of the IPMSM, it is necessary to optimize and design the IPMSM in order to meet the requirements of fully tapping the potential of the IPMSM and making the performance of the IPMSM to the extreme [3], [4], [5].

Maintaining constant power and high efficiency in a wide speed range are the main performance requirements of IPMSM for electric vehicles. When the IPMSM runs with high speed, that is, under the deep flux weakening condition, the frequency increases with the increment of the speed, and the iron loss has the greatest impact on the total efficiency. Eddy loss is dominant in the iron loss of the IPMSM including eddy loss and hysteresis loss. In this case, the amplitude of the fundamental air-gap flux density becomes smaller, and the eddy loss of the stator is mainly determined by the rotor magnetomotive force (MMF) harmonics caused by the rotor flux barrier. therefore, the stator iron loss of the IPMSM is greatly affected by the rotor topology structure [6], [7], [8], [9]. The stator harmonic loss is mainly caused by the harmonic generated by the rotor permanent magnet. The stator core loss can be effectively reduced by optimizing the angle and type of the flux barrier of the double-layer permanent magnet [10]. By optimizing the type and position of the flux bridge and the flux barrier, the torque density and the ability of flux weakening speed regulation are greatly improved [11].

The IPMSM with V type rotor topology structure is designed and the pole arc angle of the V type permanent magnet is optimized. The results show that the iron loss can be effectively reduced [12]. The IPMSM with IV type rotor topology structure is optimized, the results show that the iron loss is significantly reduced after the optimization, while the average torque is only slightly reduced [13]. The iron losses of the IPMSM with V type, 2V type, 3V type and 4V type rotor topology structures under the condition of deep flux weakening are compared and analyzed, the results show that the iron losses decrease with the increment of the number of permanent magnet layers [14]. It is found that the higher the running speed, the greater the eddy loss of the permanent magnet, and the more serious the heating of the permanent magnet, which will lead to irreversible demagnetization, which is also one of the main problems of the IPMSM [15]. The torque ripple and iron loss of the IPMSM are studied, the results show that the iron loss is significantly reduced by optimizing the IPMSM, but the torque ripple is greatly increased, it is difficult to reduce the torque ripple and iron loss at the same time [16], [17].

In this paper, an IPMSM with I2V type rotor topology structure is proposed, which can achieve high torque density, low torque ripple and low iron loss at the same time.

Firstly, the waveforms of no-load air-gap flux density of the IPMSM with three different optimized rotor topology structures are analyzed and compared. The output average torque of the IPMSM with I2V type proposed in this paper versus current angle, current density and speed under different working conditions are analyzed and compared with the V and IV type rotor topology structures. The results show that the torque performance of the IPMSM with I2V type rotor topology structure is better than that of the other two rotors under different working conditions. Then, the iron loss of the IPMSM with three different optimized rotor topology structures under different working conditions are analyzed and compared. Compared with the other two rotors, the iron loss of the IPMSM with the I2V type is the smallest, the iron loss of the IPMSM with I2V type is significantly less than that of the other two rotors especially under the deep flux weakening conditions. To overcome the problem that the IPMSM with I2V type rotor topology structure proposed in this paper achieves the optimization goal of high speed with low iron loss while the torque ripple and cogging torque greatly increase, this paper proposes a simple and effective method to add a set of circular magnetic isolation holes between the second layer and the third layer of permanent magnets, and optimize and adjust the position and diameter of this set of circular magnetic isolation holes by establishing a parameterized model of magnetic isolation holes. The results show that the torque ripple and cogging torque of the IPMSM with the further optimized I2V type rotor topology structure are greatly reduced, which has great significance to reduce vibration and noise of the IPMSM. the iron loss and magnet loss of the IPMSM with the I2V type are also effectively reduced after the further optimization, which can further increase the proportion of high efficiency area of motor. Finally, the von Mises stress and the total displacement of the rotor deformation of the IPMSM with optimized I2V type rotor topology structure under different working conditions are verified by finite element analysis. The results show that the optimized I2V type rotor topology structure of the IPMSM will not rupture under different working conditions. The displacement of the rotor deformation under different working conditions is small enough to avoid the phenomenon of the touch between stator and rotor caused by excessive displacement.

II. ANALYSIS OF ELECTROMAGNETIC TORQUE AND IRON LOSS

A. ANALYSIS OF ELECTROMAGNETIC TORQUE

The vector diagram of the IPMSM in d-q coordinate system is shown in Figure 1. As shown in Figure 1, the angle between the stator current space vector i_s and the q-axis is the current angle α. The current angle is a very important variable for the IPMSM. Taking the q axis as the starting coordinate axis, the current angle with counterclockwise rotation is positive, and the current angle with clockwise rotation is negative. The positive and negative of the current angle determines the

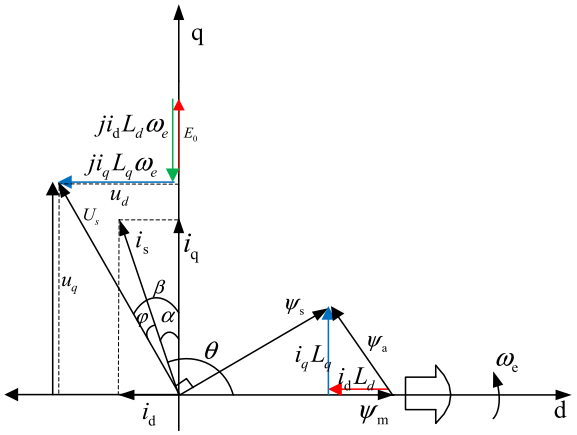

FIGURE 1. Phasor diagram of the IPMSM in d, q coordinate system.

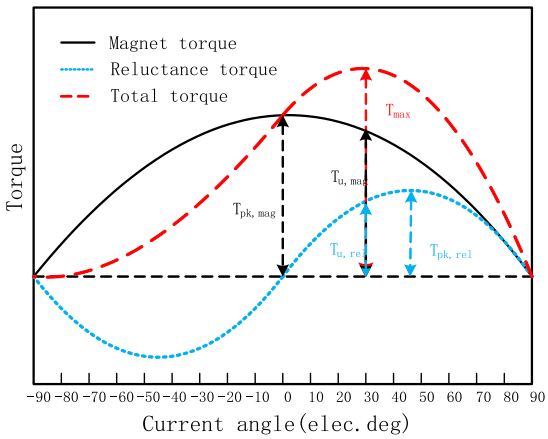

FIGURE 2. Magnet torque, reluctance torque and total torque versus current angle.

working condition of the IPMSM. When the current angle is negative, the IPMSM works in the state of magnetization, and the reluctance torque is negative. When the current angle is positive, the IPMSM works in the condition of flux weakening speed regulation, and the reluctance torque is positive. In order to make effective use of reluctance torque, improve the constant power speed range and operation efficiency of the IPMSM, the current angle is positive, the value range is 0-90°.

The flux linkage equations of the IPMSM in d, q coordinate systems can be expressed as

$$\begin{cases} \psi_d &= L_d i_d + \psi_m \\ \psi_q &= L_q i_q \end{cases} \tag{1}$$

The voltage equations of the IPMSM in d, q coordinate systems can be expressed as

$$\begin{cases} u_d &= \frac{d\psi_d}{dt} - \omega_m \psi_q + R_1 i_d \\ u_q &= \frac{d\psi_q}{dt} + \omega_m \psi_d + R_1 i_q \end{cases} \tag{2}$$

The electromagnetic torque equations of the IPMSM in d, q coordinate systems can be expressed as

$$T_e = \frac{3}{2} p \left[\psi_m i_q + (L_d - L_q) i_d i_q \right] \tag{3}$$

$$\begin{cases} i_d = -i_s \sin\alpha \\ i_q = i_s \cos\alpha \end{cases} \tag{4}$$

Based on Equations 3 and 4, the electromagnetic torque equation is further expressed as

$$T_{mag} = 1.5p * \psi_m i_s \cos\alpha \tag{5}$$

$$T_{rel} = 0.75p * (L_q - L_d) i_s^2 \sin 2\alpha \tag{6}$$

$$T_e = T_u = T_{mag} + T_{rel} \tag{7}$$

where u_d,u_q are respectively the winding voltage of d and q axis; And i_d, i_q are respectively the winding current of d and q axis, ω_m is the electrical angular velocity, L_d, L_q is the equivalent inductance of d, q axis. R_1 is the stator phase resistance, ψ_m is the synthetic flux linkage generated by the permanent magnet on the d axis and p is the pole numbers.

According to Equation 5-7, the total torque T_u mainly includes magnet torque T_{mag} and reluctance torque T_{rel}. according to Equation5-7. The total torque, magnet torque, reluctance torque versus current angle is shown in Figure 2. As shown in Figure 2, it can be found that the magnet torque takes the maximum value when the current angle is 0°, the reluctance torque takes the maximum value when the current angle is 45°, and the total torque takes the maximum value when the current angle is about 30°.

It can be further obtained from Figure 1 that the limit value of the voltage and the current are expressed as

$$\begin{cases} (L_q i_q) + (L_d i_d + \psi_m)^2 = (\frac{u_{\lim}}{\omega_m})^2 \\ i_d^2 + i_q^2 \le i_{\lim}^2 \\ U_{\lim} \ge \sqrt{u_d^2 + u_q^2} \end{cases} \tag{8}$$

When the DC bus voltage of the inverter is U_{DC}, the effective value of the maximum fundamental phase voltage can be given as

$$U_{\lim} = \frac{U_{DC}}{\sqrt{6}} \tag{9}$$

The rotor magnetic field of the IPMSM is generated by the permanent magnet, and the permanent magnet flux linkage is basically kept constant. According to Equations 8 and 9, as the angular velocity gradually increases, it is necessary to increase the amplitude and current angle to weaken the air-gap magnetic field of the IPMSM, and avoid the value of the phase voltage exceeding the limit voltage value that the inverter can provide and achieve constant power flux weakening speed regulation.

B. ANALYSIS OF IRON LOSS

The iron loss mainly includes hysteresis loss and eddy loss, and the hysteresis loss is the loss caused by repeated magnetization of core materials in the process of alternating

magnetic field. The conductor in the alternating magnetic field will generate internal induced current, namely eddy current, the higher the frequency of alternating magnetic field, the larger the eddy current. The induced eddy current energy can make the core heat and cause loss, that is, eddy loss. Additional losses are all losses except hysteresis loss and eddy current loss.

When the flux density varies sinusoidally, the Bertotti loss separation calculation model [18] is adopted, and the total loss per unit mass of core (W/kg) is expressed as

$$\begin{aligned} P_t &= P_h + P_e + P_{exc} \\ P_t &= K_h f B_m^{\delta} + K_e f^2 B_m^2 + K_{exc} f^{1.5} B_m^{1.5} \end{aligned} \tag{10}$$

where, P_h is the hysteresis loss; P_e is the eddy loss; P_{exc} is the additional loss; K_h, δ is the hysteresis loss coefficient; K_e is the eddy loss coefficient; K_{exc} is the additional loss coefficient; B_m is the peak value of flux density.

The flux density waveform of the IPMSM is generally non-sinusoidal, under a combination of alternating and rotating magnetic fields, contains a lot of harmonics [19], the iron loss can be expressed as

$$\begin{aligned} P_t &= K_{ch} K_h f B_m^{\delta} + \frac{K_e}{2\pi^2} \left(\frac{dB}{dt}\right)_{rms}^2 + \frac{K_{exc}}{(2\pi^2)^{3/4}} \left(\frac{dB}{dt}\right)_{rms}^{1.5} \\ K_{ch} &= 1 + \frac{c}{B_m} \sum_{i=1}^{N} \Delta B_i \end{aligned} \tag{11}$$

where, K_{ch} is the hysteresis loss correction coefficient considering the influence of hysteresis loop. c is a constant with a value of 0.6∼0.7, N is the number of changes in local flux density within a period, ΔB_i is the offset value of the component of the flux density waveform. $(\frac{dB}{dt})_{rms}$ is an effective value of the rate of change of flux density with respect to time within a period.

When the motor is rotating, part of the core is in the rotating magnetic field. Generally, the loss caused by the rotating magnetic field can be studied by dividing the rotating magnetic field into two orthogonal alternating magnetic fields. For the elliptic rotating magnetic field of k harmonic, it can be decomposed into two orthogonal alternating magnetic fields with long-axis magnetic flux density B_{kmax} and short-axis magnetic flux density B_{kmin}. Therefore, hysteresis loss, eddy current loss and additional loss of stator core can be expressed as

$$\begin{cases} P_h &= \sum_{k=1}^{N} K_h k f (B_{k\max}^{\alpha} + B_{k\min}^{\alpha}) \\ P_e &= K_e \sum_{i=1}^{N} K_e k^2 f^2 (B_{k\max}^2 + B_{k\min}^2) \\ P_{exc} &= K_{exc} \frac{1}{T} \int_0^T \left| \left| \frac{dB_r(t)}{dt} \right|^2 + \left| \frac{dB_t(t)}{dt} \right|^2 \right|^2 dt \end{cases} \tag{12}$$

where, B_r and B_t are respectively radial and tangential flux densities in the iron core. On this basis, the flux density waveform of each subdivision element in the stator core is obtained by time-step finite element method, and the iron loss of the corresponding part can be obtained according to equation (10-12), and the total iron loss can be obtained by the summation.

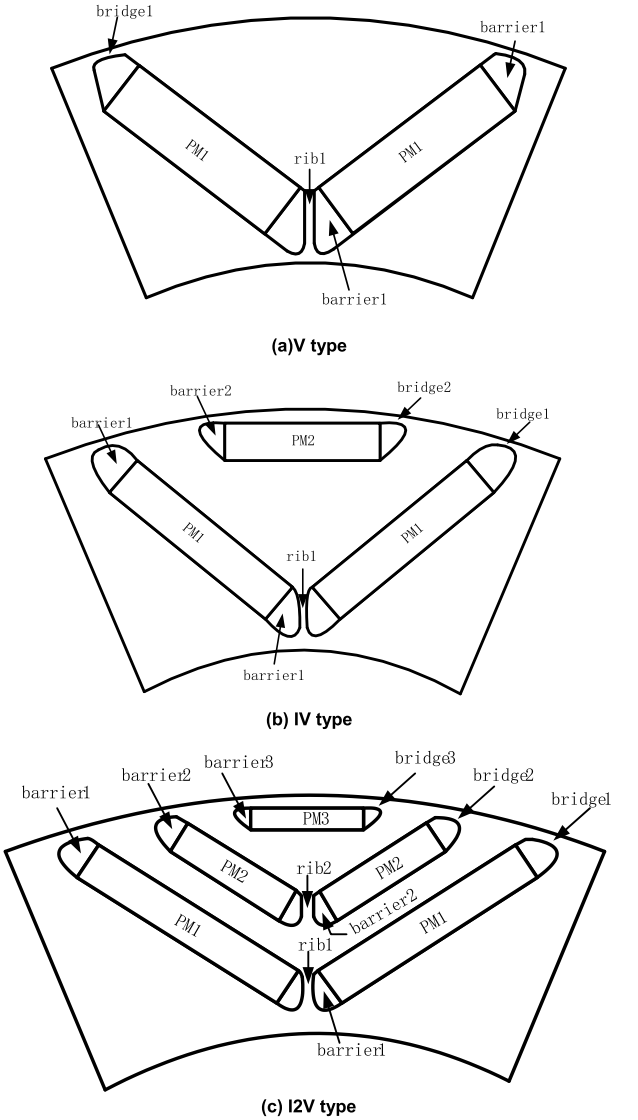

FIGURE 3. The IPMSM with different rotor topology structures.

It can be found from the above analysis that the iron loss is mainly determined by the frequency (speed), and then related to the amplitude and harmonic contents of the flux density, and the variation of local flux density in one period. Under the condition that the frequency of the motor is fixed, increasing the sinusoidal degree of the waveform of the air-gap flux density is an effective method to reduce the iron loss.

III. THE CHARACTERISTICS AND ROTOR TOPOLOGY STRUCTURE OPTIMIZATION OF THE IPMSM

A. THE CHARACTERISTICS OF THE IPMSM

Three different rotor topology structures of the IPMSM with the I2V type proposed in this paper and the V type, IV type are shown in Figure 3. As shown in Figure 3, it can be found that the rotor structure is mainly composed of rotor core,

TABLE 1. Motor characteristics.

Design parameters	Value
Rated power	110kW
Peak power	180kW
Rated speed	6000r/min
Maximum speed	16000r/min
DC bus voltage	600V
Phase	3phases
poles	8poles
Number of stator teeth	48(distributed)
Stator materials	M250-35A
Rotor materials	M250-35A
N38UH（20℃）	Br=1.26T,Hc=-954930A/m
Diameter of stator	220mm
Diameter of rotor	142.5mm
The length of air gap	0.7mm
Continuous phase current amplitude	300A
Maximum phase current amplitude	500A

flux barrier, flux bridge, ribs between permanent magnets, and permanent magnets at each layer. The total mass of rotor permanent magnets of the three kinds of rotor topology structures are basically the same, while the consumption of permanent magnets of the I2V type rotor topology structures is slightly reduced, and the same stator is adopted. For rotor topology structure of one pole, V type has two permanent magnets, IV type has three permanent magnets, and I2V type has five permanent magnets.

The characteristics of the investigated IPMSM is shown in Table 1. The number of rotor poles, stator slots is matched with 8 poles and 48 slots with the distributed windings aiming to reduce the 5th and 7th harmonics. The amplitude of continuous phase current is 300 A, and its current density is 9.6A/mm^2, the amplitude of maximum phase current is 500 A, and its current density is 16.0 A/mm^2. The IPMSM are fluid cooled.

B. THE OPTIMIZATION OF ROTOR TOPOLOGY STRUC-TURE OF THE IPMSM

Since the flux density at the flux bridge is highly saturated, the harmonic contents of the air-gap flux density are mainly determined by the rotor topology structure. If the rotor topology structure is not optimized, the harmonic contents of the air-gap flux density will be increased. When the IPMSM is running at high speed, the frequency of the fluctuation of the flux density amplitude of these harmonics in the stator core becomes larger, leading to a rapid increase in iron loss and a significant reduction in efficiency [20]. It can be concluded that increasing the layer number of permanent magnet can effectively improve the sinusoidal degree of the waveform of the air-gap flux density and no load back EMF, and reduce the harmonic contents [14], [21], which can greatly reduce the iron loss and improve the efficiency and control accuracy of the IPMSM.

The air-gap flux density and the harmonic contents of no-load back EMF waveform are mainly determined by the rotor

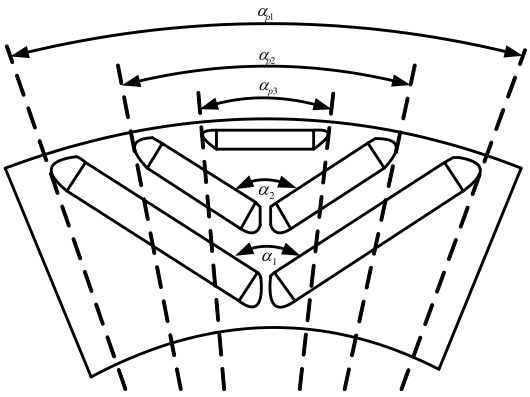

FIGURE 4. The Schematic of rotor topology parameters.

topology structure. As shown in Figure 4, so it is necessary to optimize the rotor topology structure of the IPMSM. Therefore, it is significant to optimize and analyze the mechanical opening angle and the pole-arc electric angle of each layer permanent magnet to improve the sinusoidal degree of the waveform of the air gap flux density and no-load back EMF, reduce harmonic contents and iron loss, and improve operation efficiency and control accuracy of the IPMSM. The pole arc angle of the first layer permanent magnet (The PM1 pole-arc Angle) has the greatest influence on the performance of the IPMSM, so this paper mainly analyzes and optimizes the parameter of the PM1 pole-arc Angle.

The influence of the PM1 pole-arc Angle on the performance of the IPMSM with three different rotor topology structures is shown in Figure 5. As shown in Figure 5(a), it can be found that when the PM1 pole-arc Angle of the IPMSM with three different rotor topology structures is set to 130°, the harmonic distortion of no-load back EMF can reach the minimum value. The smaller the harmonic distortion of no-load back EMF, the higher the control accuracy and the smaller the iron loss caused by harmonic.

Under rated working conditions with speed of 6000rpm, current amplitude of 300A and current angle of 30°, the output average torque of the IPMSM with three different rotor topology structures versus the PM1 pole-arc Angle is shown in Figure 5(b). As shown in Figure 5(b), the output average torque gradually decreases with the increment of the PM1 pole-arc Angle α_{p1} and the output average torque of the IPMSM with I2V type rotor topology structure proposed in this paper decreases relatively slowly. Under deep flux weakening conditions with speed of 16000rpm, current amplitude of 500A and current angle of 80°, the iron loss of the IPMSM versus the PM1 pole-arc Angle is shown in Figure 5(c). As shown in Figure 5(c), it can be found that the iron loss of the IPMSM gradually decreases with the increment of the PM1 pole-arc Angle, and the iron loss of the IPMSM with I2V type rotor topology structure proposed in this paper decreases the fastest. As shown in Figure 5(b) and (c), it can draw the conclusions that as the PM1 pole-arc Angle is set to 130°, the output average torque and the iron loss of the IPMSM

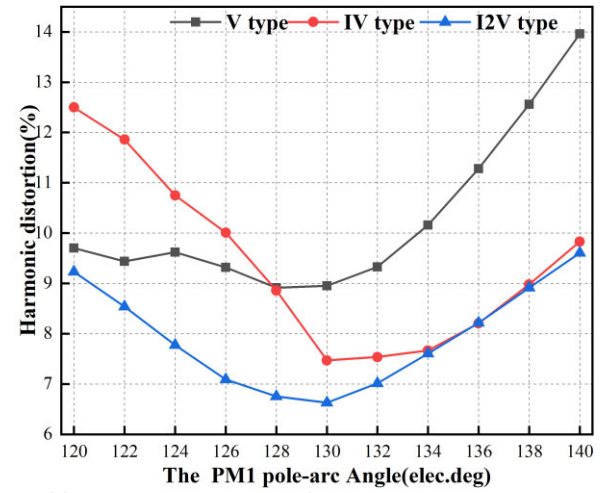

(a) The harmonic distortion of no load back EMF versus the PM1 pole-are Angle

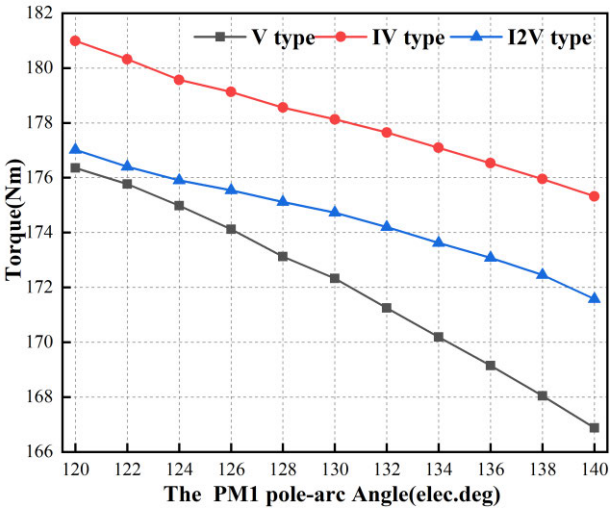

(b) The output average torque versus the PM1 pole-are Angle

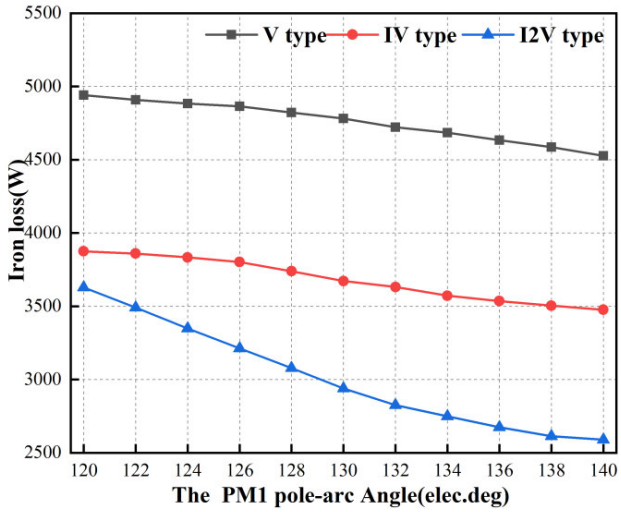

(c) The iron loss versus the PM1 pole-are Angle

FIGURE 5. The Influence on motor performance of the PM1 pole-are Angle.

can be taken into consideration simultaneously. From what has been discussed above, the PM1 pole-arc Angle of the

TABLE 2. Optimization parameters with three different rotor topologies.

Parameters	V type	IV type	I2V type
α_1(deg)	115	115	115
α_2(deg)	NAN	NAN	115
α_{p1}(elec.deg)	130	130	130
α_{p2}(elec.deg)	NAN	66	78
α_{p3}(elec.deg)	NAN	NAN	50
PMT1 (mm)	7	4.5	3.5
PMT2 (mm)	NAN	4	3
PMT3 (mm)	NAN	NAN	2
PMW1 (mm)	18	20	22
PMW2 (mm)	NAN	18	12
PMW3 (mm)	NAN	NAN	12
PMV (kg)	2.011	2.011	1.995

TABLE 3. Magnet cost of three motors(N38UH).

Parameters	V type	IV type	I2V type
Original material (dollar)	116	116	115
Manufacturing process (dollar)	25	32.5	40
Surface treatment (dollar)	3	3	3
Total (dollar)	144	151.5	158

IPMSM with different rotor topology structures is determined to be 130°.

The optimized rotor parameter values of the IPMSM with different rotor topology structures are shown in Table 2, including the opening angle of each layer of permanent magnet, the pole-arc angle of each layer of permanent magnet, the size of each layer of permanent magnet and the total mass of permanent magnet, Where PMT, PMW and PWV are the thickness of the permanent magnet, the width of the permanent magnet, the total mass of the permanent magnet respectively.

As shown in Table 2, the total volumes of the permanent magnets (N38UH) in three rotors are almost identical, so the original material cost is almost equal. The cost of magnet surface treatment (electroplating) of three kinds of motors are equal. For one polar, the I2V type has five pieces of magnets, the IV type has three pieces of magnets the V type has two pieces of magnets. As the total volumes of permanent magnet is the same, the more pieces of permanent magnet are divided, the thinner the permanent magnet is. the thinner the magnet, the higher its specific cost, therefore, the cost of magnet of I2V type and IV type is higher 60% and 30% than the V type due to manufacturing process is more complicated. The magnet cost of the IPMSM with different rotor topology structures are shown in Table 3.

For the design of the IPMSM, the optimization of no-load air gap flux density waveform is very important. Because the maximization of the amplitude of the fundamental air-gap flux density and the minimization of its THD can simultaneously achieve high torque density, low torque ripple and low iron loss of the IPMSM. After the optimization of three different rotor topology structures, the amplitude of the fundamental no-load air-gap flux density of the IPMSM is maximally increased and the THD is minimized. The optimized no-load air-gap flux density and spectral components of the IPMSM with different rotor topology structures are shown in Figure 6. As shown in Figure 6(a), it can be found that the

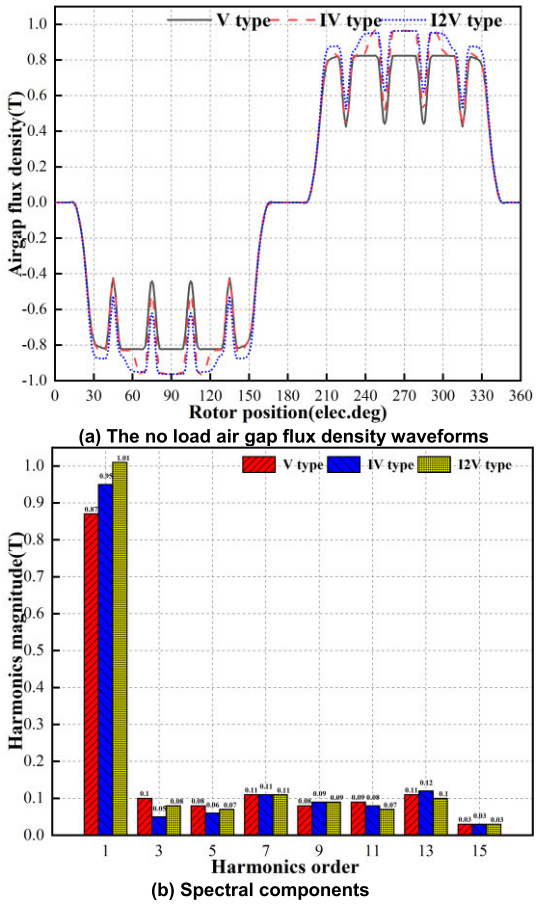

FIGURE 6. The Optimal no load air gap flux density waveforms.

TABLE 4. The amplitude of the fundamental and THD of no-load air-gap flux density with three different rotor topologies.

Parameter	V type	IV type	I2V type
THD (%)	29.2	23.1	21.5

no load air-gap flux density of the IPMSM with the I2V type rotor topology structure proposed in this paper is closer to the sinusoidal waveform. As shown in Figure 6(b), the amplitude of the fundamental no-load air-gap flux density of the IPMSM with I2V type rotor topology structure proposed in this paper is the largest. The THD of no-load air-gap flux density of the IPMSM with different rotor topology structures is shown in Table 4. As shown in Table 4, it can be found that the no load air-gap flux density waveform of the IPMSM with I2V type rotor topology structure proposed in this paper has the lowest THD and the highest sinusoidal degree, which is helpful to reduce iron loss and improve operation efficiency of the IPMSM.

IV. THE ANALYSIS AND COMPARISON OF THE FEA RESULTS FOR IPMSMS

A. THE ANALYSIS AND COMPARISON OF TORQUE PERMORMANCE OF THE IPMSMS

According to Equation 5-7, the torque of the IPMSM is mainly composed of magnet torque and reluctance torque.

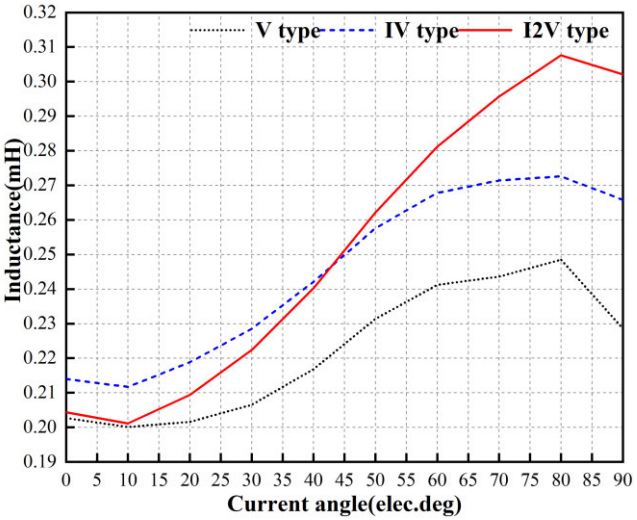

FIGURE 7. The difference between the d axis and q axis inductances versus the current angle.

The reluctance torque is proportional to the difference between the d axis and q axis inductances. The difference between the d axis and q axis inductances of the IPMSM with different rotor topology structures versus the current angle are shown in Figure 7.

Under rated working conditions with speed of 6000rpm, current amplitude of 300A, the output average torque of the IPMSM with three different rotor topologies versus the current angle are shown in Figure 8. As shown in Figure 7, it can be found that when the current angle changes in the range of 0°-45° under flux weakening conditions, the inductance difference between d and q axis of the IPMSM with IV type is the largest, as shown in Figure 8(a), at this time, the reluctance torque of the IPMSM with IV type is the largest. When the current angle changes in the range of 45°-90°, and the IPMSM is under deep flux weakening condition, the difference between the inductance of d and q axis of the IPMSM with I2V type is the largest, as shown in Figure 8(a), at this time, the reluctance torque of the IPMSM with I2V type is the largest, which has more obvious advantages compared with the IPMSM with V type. The higher the utilization rate of the reluctance torque under the deep flux weakening condition, the greater the high efficiency operating range of the IPMSM.

As shown in Figure 8(b), it can be found that when the current angle is running in the range of 0°-60° under flux weakening conditions, the magnet torque of the IPMSM with I2V type is the largest, which has more obvious advantages compared with V type. When the current angle is running in the range of 60°-90° under deep flux weakening conditions, the magnet torque of the IPMSM with IV type is the largest, but compared with the IPMSM with V type the advantages are not obvious.

As shown in Figure 8(c), it can be found that when the current angle is running in the range of 0°-90° under flux weakening conditions, the total torque of the IPMSM with

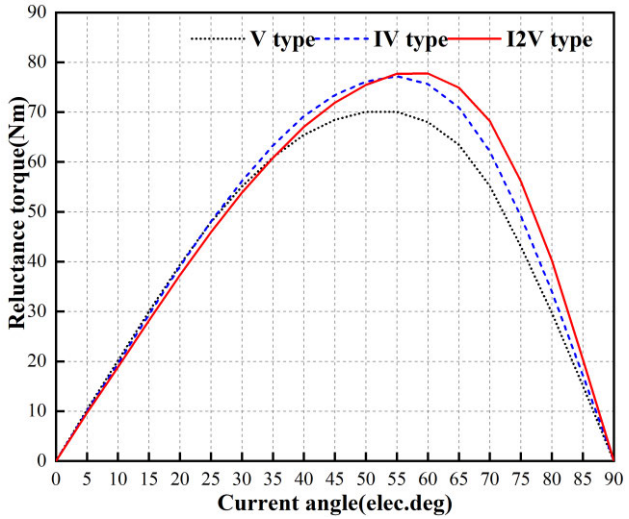

(a)The reluctance torque versus current angle

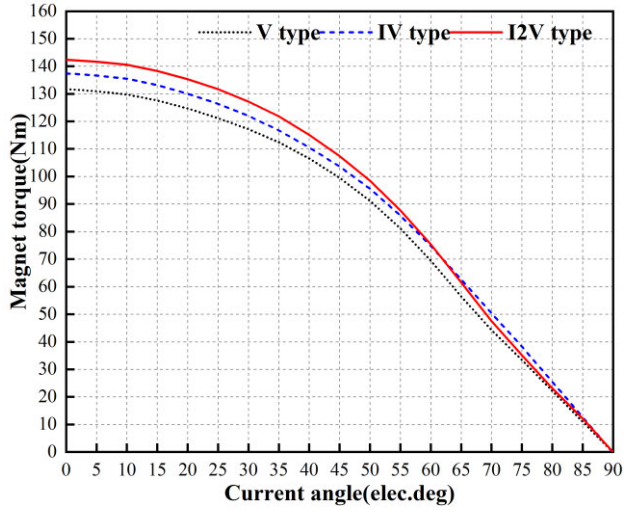

(b)The magnet torque versus current angle

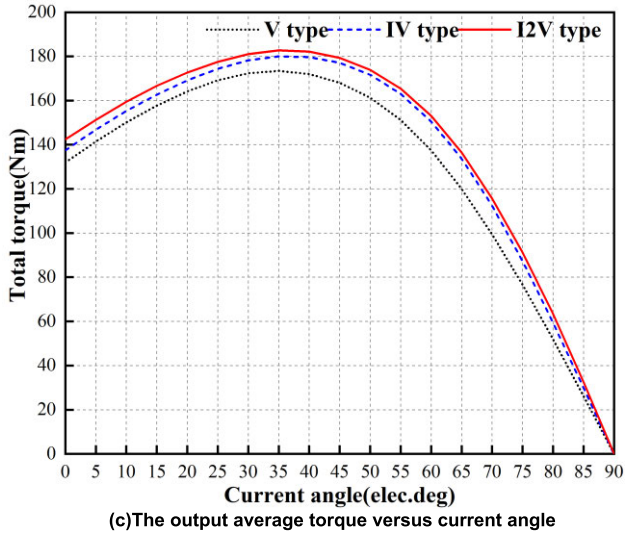

(c)The output average torque versus current angle

FIGURE 8. The comparison of output torque with three different rotors.

I2V type consisting of magnet torque and reluctance torque is always larger than the other two types, that is to say, the torque performance of the IPMSM with I2V type proposed

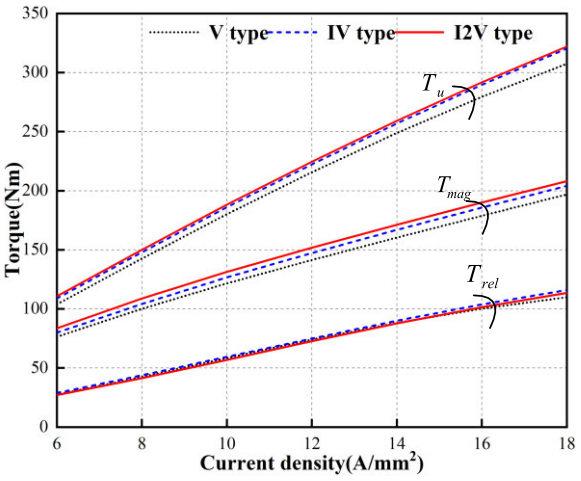

(a)The current angle with 30°

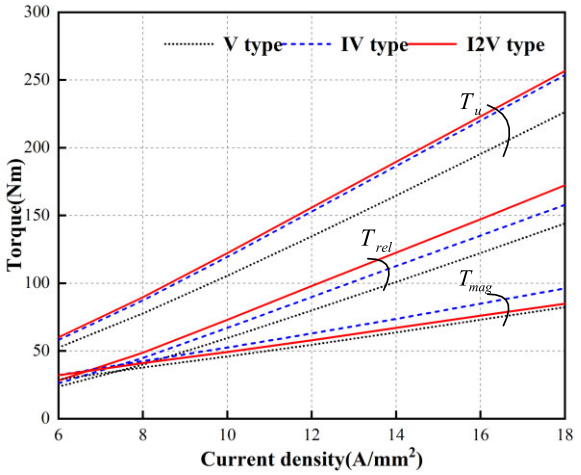

(b)The current angle with 70°

FIGURE 9. The output torque versus current density with different current angle.

in this paper is better than that of the other two rotor topology structures under the whole flux weakening speed regulation conditions.

The output torque versus current density at different current angles is shown in Figure 9. As shown in Figure 9, it can be found that the total output average torque increases with the increment of the current density. The output total average torque of the IPMSM with I2V type proposed in this paper is larger than the other two rotor topology structures under different current densities. As shown in Figure 9(a), when the current angle is 30° under the flux weakening condition, the magnet torque of the IPMSM with I2V type proposed in this paper is significantly larger than that of the other two different rotor topology structures under different current densities. As shown in Figure 9(b), when the current angle is 70° under the deep flux weakening condition, the reluctance torque of the IPMSM with I2V type proposed in this paper is significantly larger than that of the other two different rotor topology structures under different current densities, which is consistent with the previous analysis results.

The essence of the flux weakening control is to increase the amplitude of drive current and current angle of the IPMSM, Thus, the voltage in the q-axis generated by the d-axis current component is increased to offset the growing no-load back EMF in the q-axis generated by the d-axis permanent magnet flux linkage with the increment of speed, which ensure that the resultant voltage does not exceed the maximum limit voltage that the inverter can output, and can expand the range of constant power speed regulation as far as possible. The output average torque and power versus speeds with the flux weakening condition are shown in Figure 10 and Figure 11. Figure.10 shows the comparison of the average torque of the IPMSM with three different rotor topology structures versus speed under the condition of flux weakening speed regulation, when the amplitude of current is 260A. The comparison of output average torque versus speed is shown in Fig.10(a). As shown in Fig.10(a), it can be found that when the speed is in the range of 0-8000rpm, the IPMSM with different rotor topology structures maintain constant output torque. the output average torque of the IPMSM with I2V type rotor topology structure is the largest and the V type rotor topology structure is the smallest. When the speed is higher than 8000rpm, with the increment of the speed, the back EMF value of the IPMSM with the I2V type rotor topology structure is significantly higher than that of the other two rotor topology structures, so the required demagnetization current is increasing while the total current is constant. The greater the demagnetization current, the smaller the current that can produce the torque, which lead to the output average torque of the IPMSM with I2V type rotor topology structure decreases the fastest when the IPMSM is running at high speed.

As shown in Fig.10(b), it can be seen that when the speed is in the range of 0-8000rpm, the output power of the IPMSM with different rotor topology structures are all proportional to the speed. the output average torque of the IPMSM with the I2V rotor topology structure is the largest, so its output power is also greater than the other two rotor topology structures. When the speed is in the range of 8000-10000rpm, the output power of the IPMSM with different rotor topology structures can basically maintain constant. When the speed is higher than 10000rpm, because the amplitude of current is too small with flux weakening condition, the IPMSM with different rotor topology structures cannot achieve constant power speed regulation. The main reasons are as follows: when the speed is higher than 10000rpm, the amplitude of the no-load back EMF becomes larger and larger with the further increment of the speed, it can be found from the previous analysis that in order to avoid the resultant voltage exceeding the limit voltage provided by the inverter, the current angle can only be increased to realize the deep flux weakening control. Since the torque of the IPMSM with the I2V rotor topology structure decreases the fastest, the power also decreases the fastest.

Figure.11 shows the comparison of the average torque and power of the IPMSM with three different rotor topology structures versus speed when the amplitude of current is

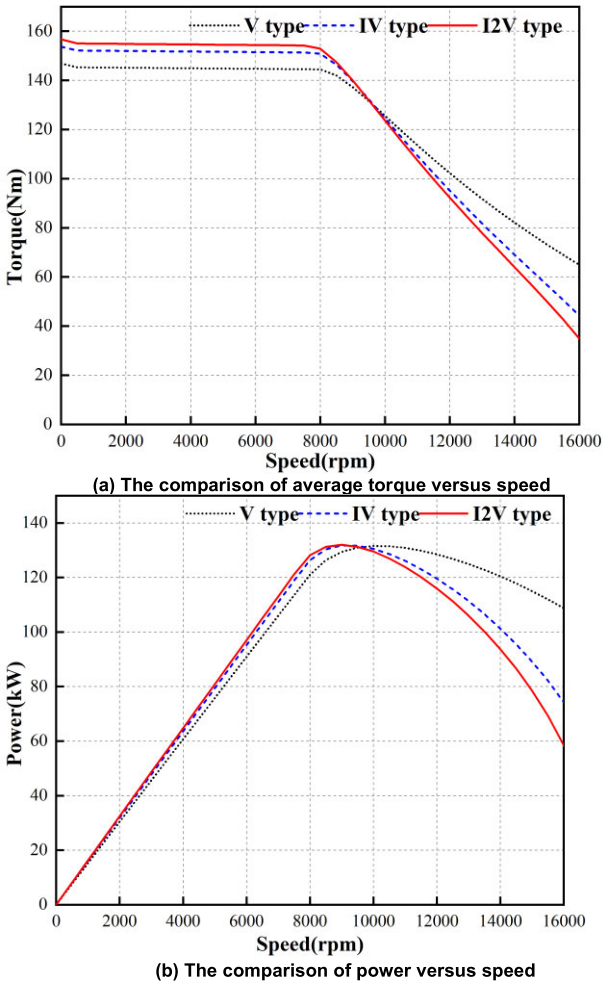

FIGURE 10. The comparison of average torque, power versus speed with three different rotor topology structures.

500A. The comparison of output average torque versus speed is shown in Figure.11(a). As shown in Figure.11(a), it can be found that the output average torque of the IPMSM with I2V type rotor topology structure proposed in this paper is greater than that of the other two shape rotor topology structures in the whole range of flux weakening speed regulation.

As shown in Figure.11(b), it can be found that when the speed is in the range of 0-7000rpm, the output power of the IPMSM with different topology structures are all proportional to the speed as the output average torque of the IPMSM with different rotor topology structures remains constant. The IPMSM with different rotor topology structures maintain constant output power when operating in the range of 8000-16000rpm.The IPMSM with different rotor topology structures maintain constant output power when operating in the range of 8000-16000rpm.Since the output torque of the IPMSM with I2V rotor topology structure is the largest in the whole flux weakening speed regulation, its output power is also greater than that of the other two rotor topology structures in the whole flux weakening speed regulation.

Under rated working conditions with speed of 6000rpm, current amplitude of 300A and current angle of 30°, The

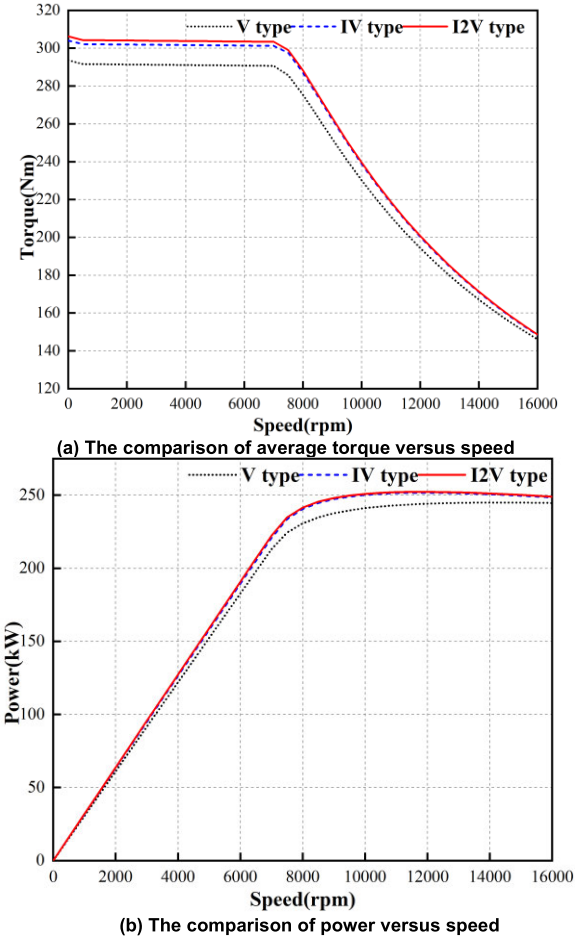

FIGURE 11. The comparison of average torque, power versus speed with three different rotor topology structures.

output torque waveforms of the IPMSM with three different rotor topology structures are shown in Figure 12. As shown in Figure 12, it can be found that the output average torque of the IPMSM with I2V rotor topology structure is the largest, and the output average torque of the IPMSM with V type rotor topology structure is the smallest. The torque ripple of the IPMSM with IV rotor topology structure is the smallest, and the torque ripple of the IPMSM with I2V type rotor topology structure is the largest.

The average torque and torque ripple of the IPMSM with three different rotor topology structures are shown in Table 5. Where T_{av} are the average torque, T_{rip} are the torque ripple. It can be clearly seen from Table 5 that the output average torque of the IPMSM with I2V rotor topology structure is the largest. Compared with the IPMSM with V type rotor topology structure, the output average torque of the IPMSM with I2V rotor topology structure is increased by 8.8Nm, with an increase of 5.11%, while the amount of permanent magnet is slightly reduced. The torque ripple and the ratio of torque ripple of the IPMSM with IV rotor topology structure are the smallest. The torque ripple and the ratio of torque ripple of the IPMSM with I2V rotor topology structure are the largest.

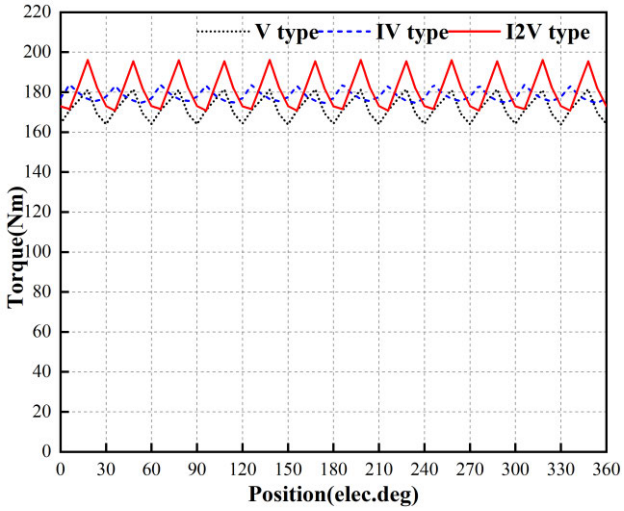

FIGURE 12. The Comparison of output torque waveforms under rated conditions.

TABLE 5. The average torque and torque ripple of the IPMSM with three different rotor topologies.

Parameter	V type	IV type	I2V type
T_{av} (Nm)	172.3	178.1	181.1
T_{rip} (Nm)	17.30	9.13	24.86
T_{rip} (%)	10.04	5.13	13.74

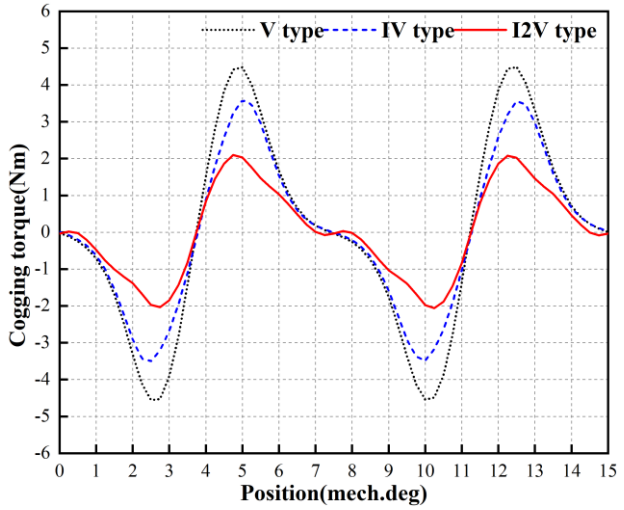

FIGURE 13. The comparison of the cogging torque waveforms under rated conditions.

The waveforms of the cogging torque of the IPMSM with different rotor topology structures under rated conditions are shown in Figure 13. As shown in Figure 13, it can be found that the cogging torque of IPMSM with I2V type rotor topology structure is the largest while the cogging torque of the IPMSM with IV type rotor topology structure is the smallest. The peak-to-peak value of the cogging torque with IV type rotor topology structure is the smallest, while the peak-to-

TABLE 6. The Comparison of average iron loss under rated conditions.

Parameter	V type	IV type	I2Vtype
W_{iron} (W)	885.58	899.92	841.11
W_{eddy} (W)	450.88	460.97	430.21
W_{hyst} (W)	434.68	439.07	410.94

TABLE 7. The Comparison of the average iron loss under deep flux weakening conditions.

Parameter	V type	IV type	I2V type
W_{iron} (W)	6425.7	4453.3	2959.2
W_{eddy} (W)	5627.9	3923.0	2534.5
W_{hyst} (W)	799.0	526.5	418.1

peak value of the cogging torque with I2V type rotor topology structure is the largest.

The above simulation result can find that the torque ripple and cogging torque of the IPMSM with I2V type rotor topology structure proposed in this paper are all the largest, which will lead to the operating vibration and noise. Therefore, it is necessary to further optimize the I2V type rotor topology structure proposed in this paper to reduce the torque ripple and the cogging torque.

B. THE ANALYSIS AND COMPARISON OF THE IRON LOSS AND EFFICIENCY OF THE IPMSMS

Iron loss is the main component of the loss of the IPMSM under the condition of flux weakening conditions with high speed. The iron loss is mainly determined by the frequency or speed of the IPMSM, and the iron loss is also related to the amplitude of flux density through the stator and rotor of the IPMSM, harmonic content and the variation of local flux density in a period. Figure 14 shows the comparison of loss of the IPMSM with different rotor topology structures under rated working conditions. The average eddy loss W_{eddy}, average hysteresis loss W_{hyst} and total average iron loss W_{iron} of the IPMSM with three different rotor topology structures obtained from Figure 14 are shown in Table 6. It can be clearly seen from Table 6 that under rated working conditions, the total iron loss of the IPMSM with the I2V rotor topology structure proposed in this paper is the smallest, compared with IV type rotor topology structure, the average iron loss of the IPMSM with I2V rotor topology structure proposed in this paper is reduced by 58.81W, with a reduction of 6.5%.

As shown in Figure 14(d), it can be found that compared with the other two type rotor topology structures, the magnet loss of the IPMSM with the I2V rotor topology structure proposed in this paper is the largest, which is mainly because as the total volumes of permanent magnet of the three rotors are almost the same, the more pieces of magnet are divided, the thinner each piece of permanent magnet is. The thinner each piece of permanent magnet, the greater the magnet loss.

Under deep flux weakening conditions with speed of 16000rpm, current amplitude of 500A and current angle of 80°, The loss of the IPMSM with different rotor topology structures are shown in Figure 15. The average eddy loss W_{eddy}, average hysteresis loss W_{hyst} and total average iron loss W_{iron} of the IPMSM with three different rotor topology structures obtained from Figure 15 are shown in Table 7. It can be clearly seen from Table 7 that under the deep flux weakening condition, compared with the IPMSM with V type rotor topology structure, the total average iron loss of the IPMSM with I2V type rotor topology structure is significantly reduced by 3466.5W, with a reduction of 53.9%, which greatly improves the operation efficiency of the IPMSM with high speed.

As shown in Figure 15(d), it can be found that compared with the other two type rotor topology structures, the magnet loss of the IPMSM with the I2V rotor topology structure proposed in this paper is also the largest and the rotor topology should be further optimized to effectively reduce the magnet loss of the IPMSM with the I2V rotor topology structure in the future research.

The iron loss of the IPMSM is mainly determined by the speed or the frequency, so it is necessary to analyze and compare the relationship between the iron loss and speed. When the current amplitude is 260A, the iron loss of the IPMSM with different rotor topology structures versus speed under flux weakening control strategy are shown in Figure 16.

When the current amplitude is 500A, the iron loss of the IPMSM with different rotor topology structures versus speed under flux weakening control strategy are shown in Figure 17.

As shown in Figure 16 and Figure 17, it can be found that the eddy loss, hysteresis loss and total iron loss of the IPMSM increase with the increment of the speed. In the range of low speed with 0-8000rpm, the IPMSM is running under the control strategy of the maximum torque per ampere (MTPA), the eddy loss, hysteresis loss and total iron loss of the IPMSM with three different rotor topology structures are basically the same. However, in the range of high speed with8000-16000rpm, the IPMSM runs in deep flux weakening under the control strategy of the maximum torque per voltage (MTPV). With the increment of speed, the eddy loss, hysteresis loss and total iron loss of the IPMSM with I2V rotor topology structure is obviously lower than those of the other two rotor topology structures. The higher the speed, the more obvious the difference of the iron loss, which make the IPMSM with the I2V type rotor topology structure proposed in this paper can maintain high operating efficiency under deep flux weakening condition with high speed.

The operating efficiency versus speed of the IPMSM with three different rotor topology structures is shown in Figure 18. According to Figure 18, it can be found that when the speed is 0-8000rpm, the efficiency of the IPMSM with different rotor topology structures are all the highest. Compared with the other two rotor topology structures, the efficiency of the IPMSM with the I2V type rotor topology structure proposed in this paper is higher than that of the other two rotor topology structures when running with low speed, but the difference of the efficiency is not obvious. Since the iron loss of the

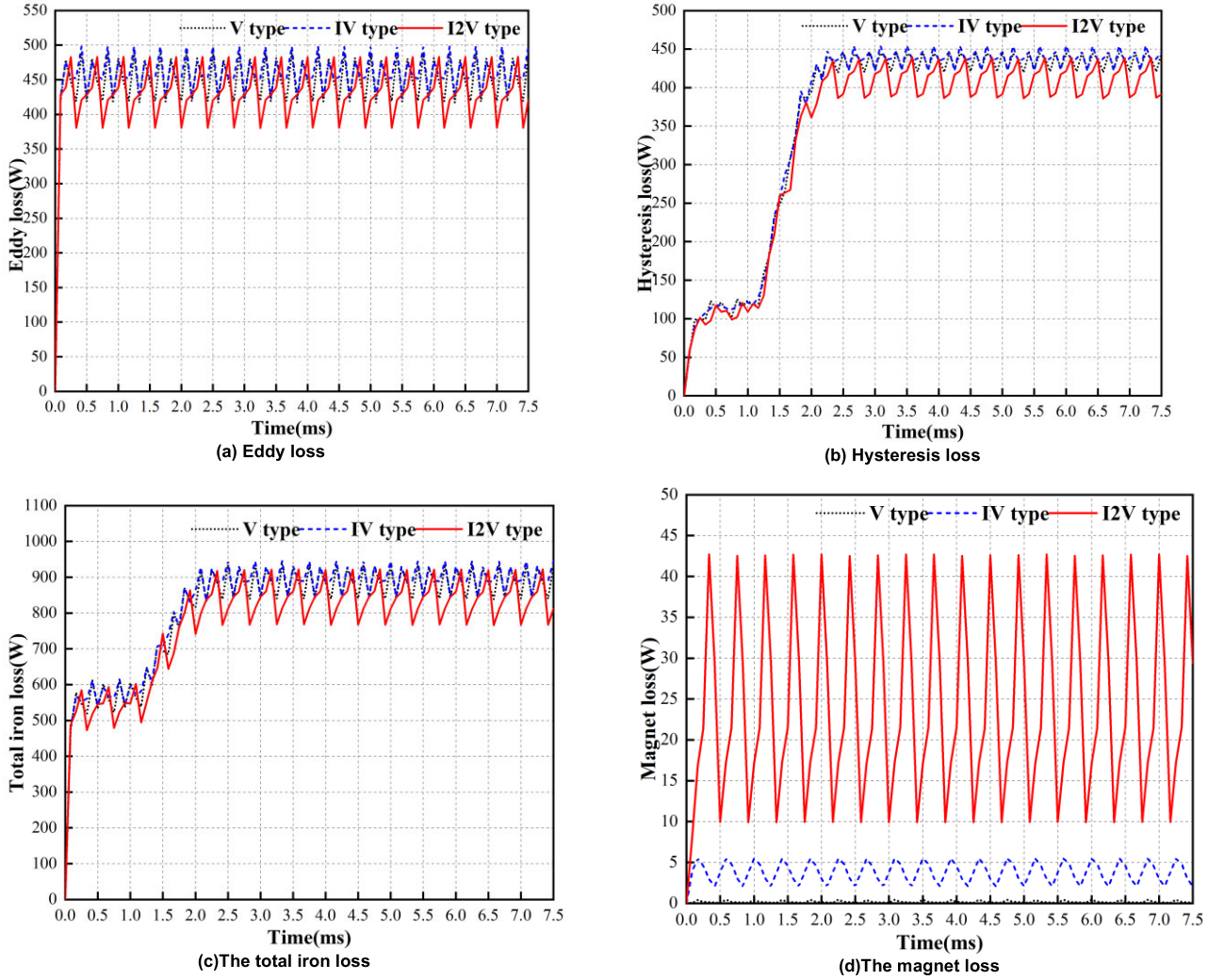

FIGURE 14. The comparison of iron loss under rated conditions.

IPMSM with I2V type rotor topology structure is significantly lower than that of the other two rotor topology structure when running under deep flux weakening conditions with high speed. Therefore, when running with high speed, the efficiency of the IPMSM with the I2V type rotor topology structure proposed in this paper is significantly higher than that of the other two rotor topology structures. The higher the speed, the more obvious difference of the efficiency between the I2V type rotor topology structure proposed in this paper and the other two rotor topology structures.

The efficiency contour maps of three IPMSMs are shown in Figure 19. As shown in Figure 19, it can be found that the high efficiency operation area of the IPMSM with I2V type rotor topology structure proposed in this paper is significantly larger than that of the other two rotor topology structures. The comparison of proportion of high efficiency areas of the three IPMSMs are shown in Table 8. As shown in Table 8, it can be found that the proportion of high efficiency areas of the IPMSM with the I2V type rotor topology proposed in this paper is the largest. Compared with the V type rotor topology structure, the proportion of high efficiency areas of the IPMSM with the I2V type rotor topology proposed in this paper greater than 97% increased by 6.32 percentage points, and the proportion of high efficiency areas of the IPMSM with the I2V type rotor topology proposed in this paper greater than 96% increased by 2.95 percentage points.

TABLE 8. Comparison of proportion of high efficiency area.

Parameter	V type	IV type	I2V type
Efficiency Above 97%	33.08%	34.80%	39.40%
Efficiency Above 96%	60.58%	61.78%	63.53%
Efficiency Above 95%	72.94%	72.55%	73.59%

C. THE FURTHER OPTIMIZATION OF ROTOR TOPOLO- GY WITH I2V TYPE

When the motor is connected with the transmission equipment to output power, the vibration of the system will increase due to the torque ripple, Therefore, it's very important to

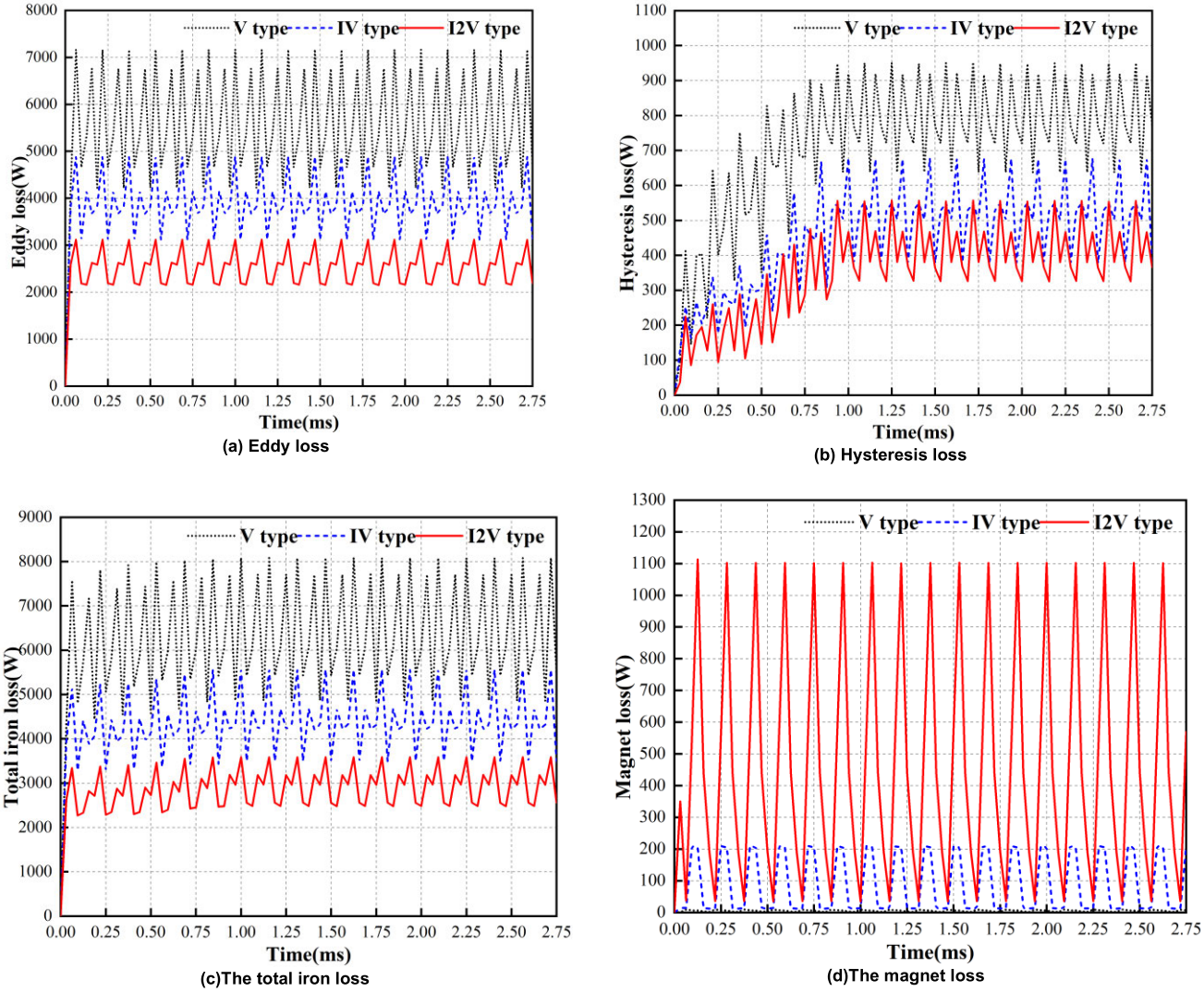

FIGURE 15. The comparison of iron loss under deep flux weakening conditions.

reduce the torque ripple of in the design process [22]. The stator skew is the most common method to reduce torque ripple [23], this method is simple in principle and has been proved to be effective in long-term industrial application, however, the stator skew increases the difficulty of embedding and winding wires, in addition, the axial unbalanced magnetic tension introduced by the stator skew will be applied to the bearing and shorten the longevity of the bearing. The stator or rotor auxiliary slot method [24], the optimization of pole-arc coefficient [25] and the permanent magnet combined with unequal pole-arc coefficient [26] were proposed in some literatures, these methods have been proved to be effective in reducing torque ripple under specific conditions, but they have not been widely used in current electric vehicles due to factors such as processing cost, technology maturity, and electro-magnetic performance degradation.

As mentioned above, the torque ripple and cogging torque of the IPMSM with the I2V type rotor topology structure proposed in this paper are much larger than those of the other two rotor topology structures, so the IPMSM with the I2V type rotor topology structure proposed in this paper needs to be further optimized. This paper proposes a simple and effective method to reduce torque ripple and cogging torque by adding a set of circular flux isolation holes between the second layer and the third layer of permanent magnets, and the position and diameter of this set of circular flux isolation holes are optimized and adjusted by establishing a parameterized model of circular magnetic isolation holes. The schematic diagram of the position and structure of the magnetic isolation hole under one pole of the IPMSM with the I2V type rotor topology structure proposed in this paper is shown in Figure 20. Firstly, the position of the magnetic isolation hole was optimized and adjusted. under the condition of ensuring the mechanical strength and the non-interference of the rotor topology structure, the distance between the center of the magnetic isolation hole and the center of the rotor

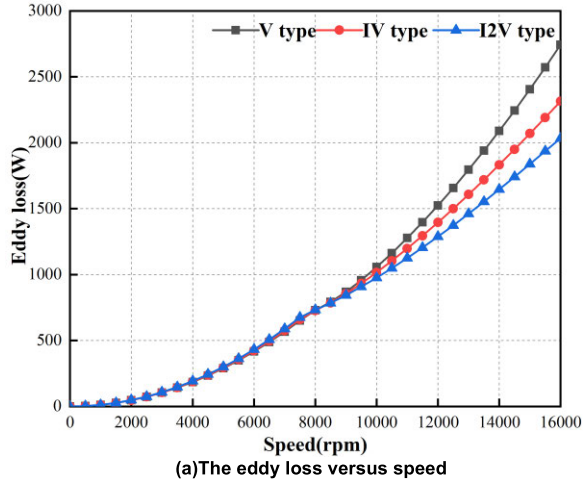

(a)The eddy loss versus speed

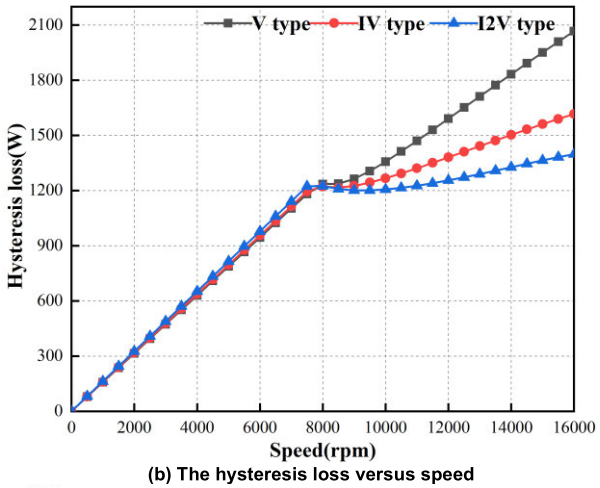

(b) The hysteresis loss versus speed

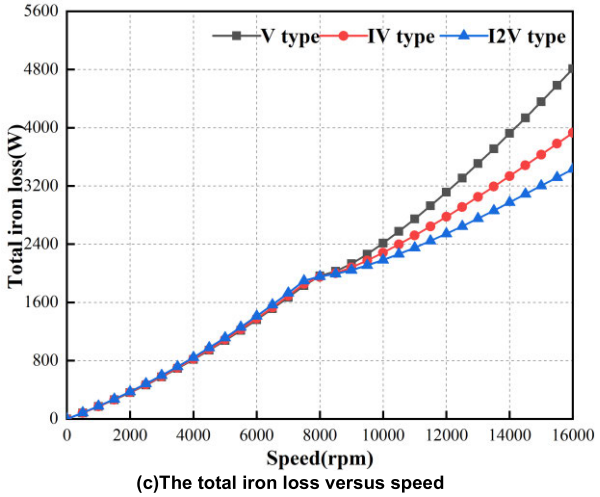

(c)The total iron loss versus speed

FIGURE 16. The iron loss versus speed under flux weakening control strategy.

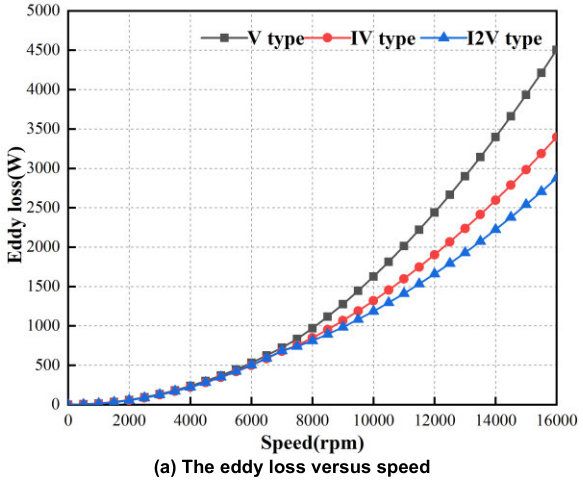

(a) The eddy loss versus speed

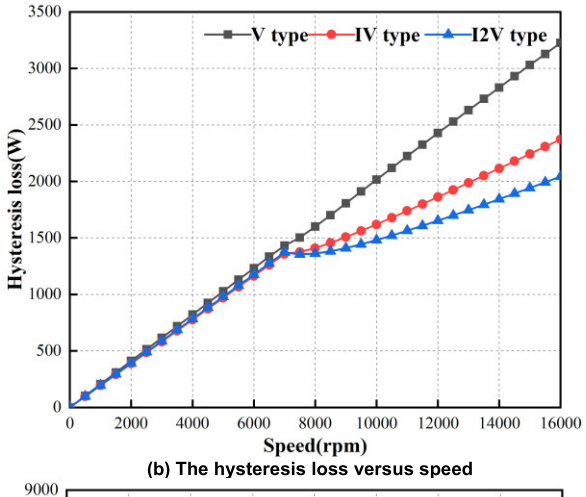

(b) The hysteresis loss versus speed

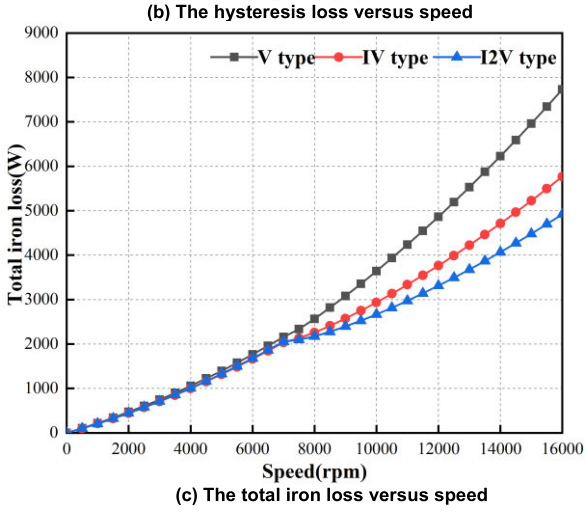

(c) The total iron loss versus speed

FIGURE 17. The iron loss versus speed under flux weakening control strategy.

was determined to be 69.25mm, and the offset angle of the magnetic isolation hole was set to be 7° after the optimization and adjustment. then, the diameter of the magnetic isolation hole is optimized and adjusted. The relationship between the output average torque, torque ripple, ratio of torque ripple and the diameter of the magnetic isolation hole is shown in Table 9. With the increment of the diameter of the magnetic isolation hole, the torque ripple is greatly reduced. When the diameter of magnetic isolation hole is 2.0mm, the torque ripple is the smallest.

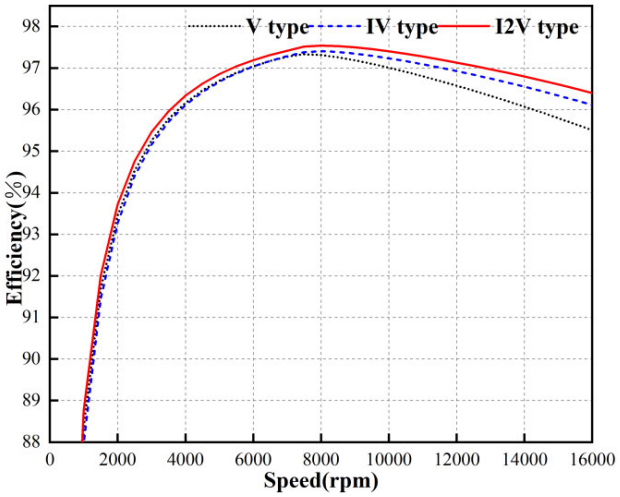

FIGURE 18. The efficiency of the IPMSM versus speed.

TABLE 9. The output average torque and torque ripple versus the diameter of the magnetic isolation hole.

Diameter (mm)	Average torque (Nm)	Torque Ripple (Nm)	Ratio of Torque Ripple (%)
1.2	181.1	18.29	10. 11
1.4	180.8	15.78	8.73
1.6	180.7	11.92	6.60
1.8	180.4	9.93	5.51
2.0	180.2	8.66	4.80

The comparison of output torque waveforms of the IPMSM with I2V type rotor topology structure after the further optimization is shown in Figure 21. As shown in Figure 21, the torque ripple of the IPMSM with I2V type rotor topology structure after the further optimization is greatly reduced, while the output average torque is reduced from 181.1Nm to 180.2Nm, which is reduced by 0.9Nm, and the reduction ratio is only 0.50%. The torque ripple value is reduced by 16.2Nm, a decrement of 65.2%. the ratio of torque ripple decreased by 8.94 percentage points from 13.74% to 4.80%, and the effect of the further optimization of the IPMSM with I2V type rotor topology structure is very obvious.

The comparison of cogging torque waveform of the IPMSM with I2V rotor topology structure after the further optimization is shown in Figure 22. As shown in Figure 22, the peak-to-peak value of the cogging torque of the IPMSM with I2V type rotor topology structure before the further optimization is 10.2Nm, and after the further optimization the peak-to-peak value of the cogging torque is 4Nm, the peak-to-peak value of the cogging torque after the further optimization is reduced by 6.2Nm, with a decrement of 60.8%. The effect of the further optimization of the cogging torque is also more obvious.

In summary, after the further optimization, the torque ripple and cogging torque of the IPMSM with the I2V type rotor topology structure are greatly reduced, which can reduce the vibration and noise of the IPMSM, and improve the ride comfort of the vehicle.

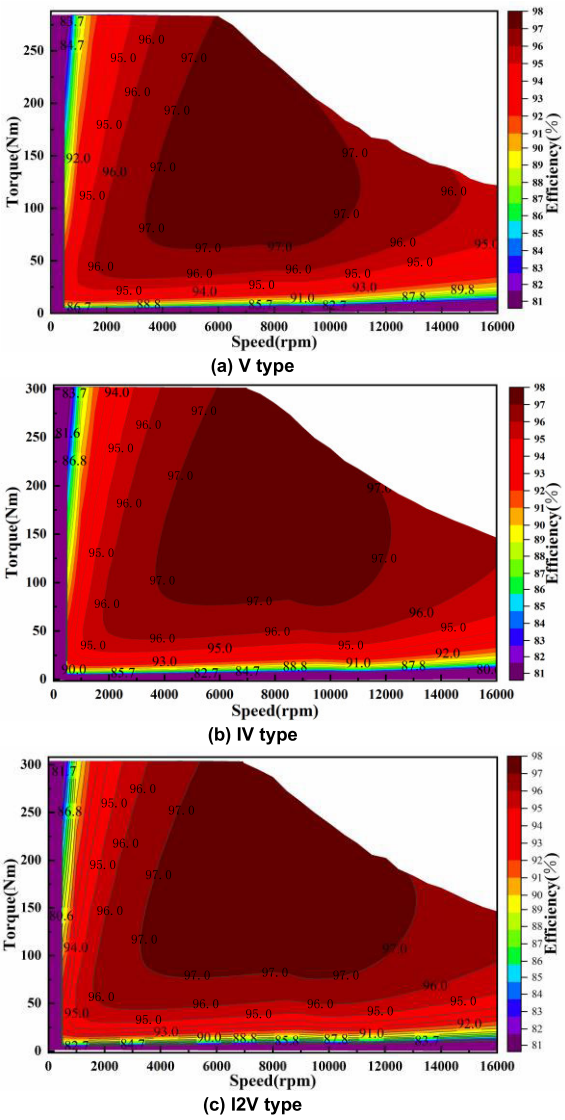

FIGURE 19. The efficiency contour maps of the IPMSMs.

Figure 23 shows the comparison of losses of the IPMSM with I2Vtype rotor topology structure after the further optimization under rated working conditions with speed of 6000rpm, current amplitude of 300A and current angle of 30°, As shown in Figure 23, it can be found that the eddy loss, hysteresis loss, total iron loss and magnet loss of the IPMSM with I2V type rotor topology structure are significantly reduced after the further optimization.

The comparison of average value of loss after the further optimization is shown in Table 10. It can be clearly seen from Table 10 that the eddy loss, hysteresis loss, total iron loss and magnet loss decrease respectively by 3W, 3.7W, 6.9W and 5.9W after the further optimization, and the optimization effect of magnet loss is the most obvious, with a decrement of 24.7%.

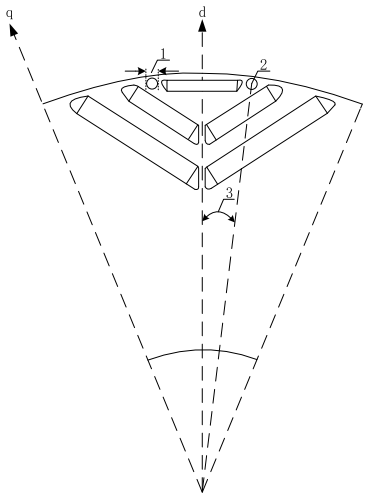

1. Diameter of magnetic isolation hole 2. Position radius of magnetic isolation hole 3. Angle between the center of the magnetic isolation hole and the d axis

FIGURE 20. The schematic diagram of the position and structure of the magnetic isolation hole with one pole.

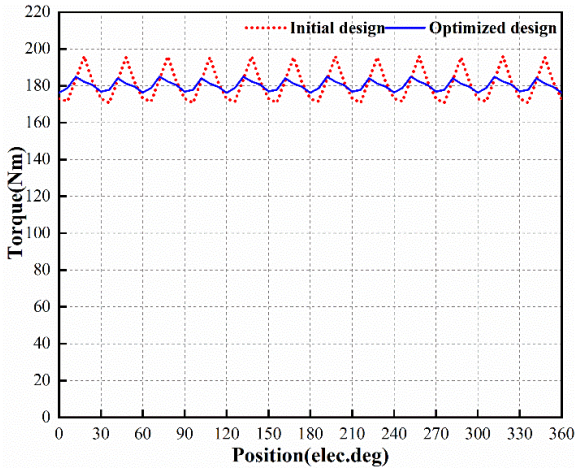

FIGURE 21. The Comparison of output torque waveforms after optimization.

TABLE 10. The Comparison of the average value of losses after the further optimization.

I2V type	Eddy loss(W)	Hysteresis loss(W)	Iron loss(W)	Magnet loss(W)
Initial design	430.2	410.9	841.1	23.9
Optimized design	427.2	407.2	834.2	18.0

Figure 24 shows the comparison of losses of the IPMSM after the further optimization under deep flux weakening working conditions with speed of 16000rpm, current amplitude of 500A and current angle of 80°, As shown in Figure 24, it can be found that the hysteresis loss, total iron loss and magnet loss of the IPMSM with I2V type rotor topology structure are all reduced after the further optimization. The comparison

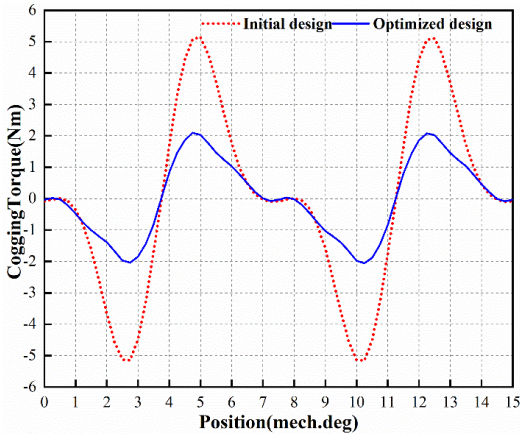

FIGURE 22. The Comparison of cogging torque waveforms after the further optimization.

TABLE 11. The Comparison of the average value of losses after the further optimization.

I2V type	Eddy loss(W)	Hysteresis loss(W)	Iron loss(W)	Magnet loss(W)
Initial design	2534.5	418.1	2954.2	467.0
Optimized design	2539.0	352.0	2891.0	451.0

of average value of losses after the further optimization is shown in Table 11, it can be found from Table 11 that after the further optimization, the hysteresis loss, total iron loss and magnet loss decrease by 66.1W, 63.2W and 6W, respectively, while the eddy loss increases by 4.5W.

To sum up, this paper proposes a simple and effective method which not only can greatly reduce the torque ripple and cogging torque of the IPMSM with I2V type while the output average torque is only reduced 0.50%, but also can further reduce the iron loss and magnet loss. The IPMSM with I2V type proposed in this paper can achieve low torque ripple, low iron loss and high torque density at the same time.

D. THE ANALYSIS AND CHECK OF MECHANICAL STRESS AND DISPLACEMENT OF THE IPMSM WITH THE FURTHER OPTIMIZED I2V TYPE ROTOR TOPOLOGY STRUCTURE

The IPMSM for electric vehicles generally has a wide speed range with constant power, and often are required to operate at high speed. When the IPMSM is operating at high speed, the rotor topology structure with the I2V type such as the bridges and center ribs and so on should be carefully designed considering both mechanical and electromagnetic characteristics. It is necessary to analyze and check whether the stress and the displacement of mechanical deformation of the rotor meet the requirements when operating with high speed. The material [27], [28] properties of rotor are shown in Table 12.

The results of finite element analysis (FEA)von Mises stress of rotor under different working conditions are shown in Figure 25. Figure 25(a) shows the von Mises stress distribution diagram of the rotor when the speed is 18000rpm.

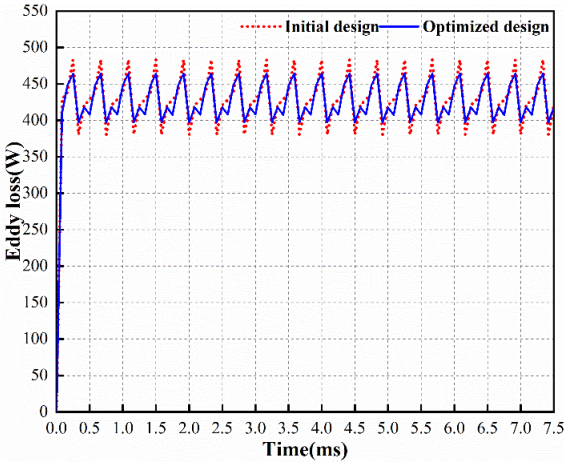

(a)The Comparison of the eddy loss

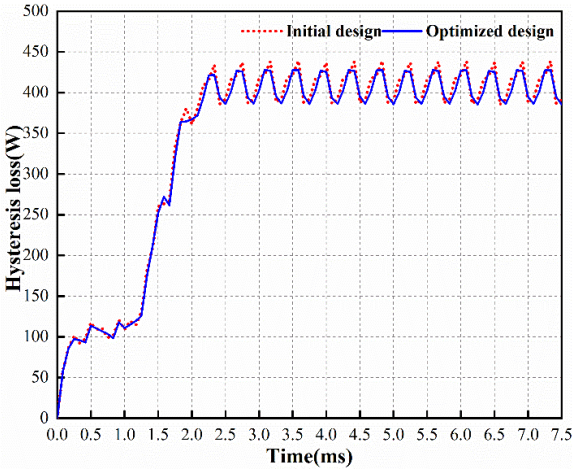

(b) The Comparison of the hysteresis loss

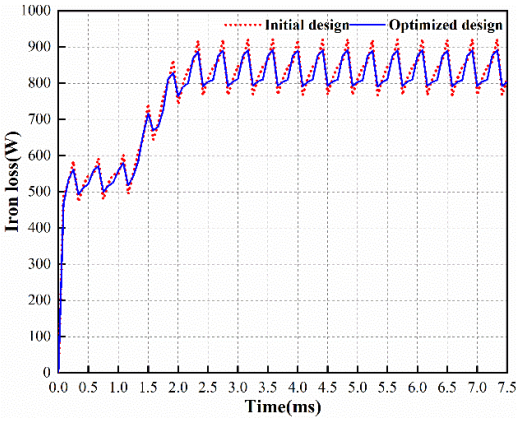

(c) The Comparison of the total iron loss

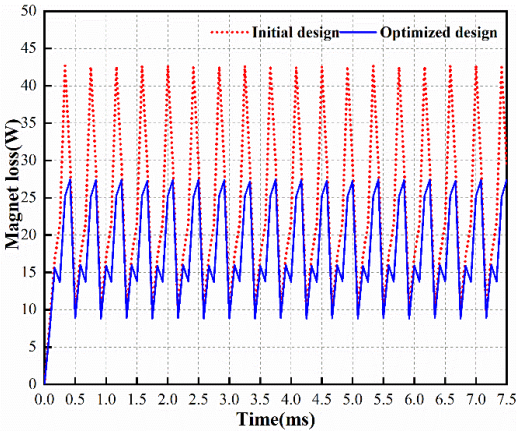

(d) The Comparison of the magnet loss

FIGURE 23. The Comparison of the iron loss of the IPMSM under rated conditions after the further optimization.

TABLE 12. The material properties of rotor.

Parameters	Steel
Young's modulus (GPa)	185
Density (kg/m^3)	7650
Poisson's ratio	0.3
Yield strength (MPa)	455

It can be found that the maximum mechanical stress points of the IPMSM with optimized I2V rotor topology structure is located on the junctions of rib1. The value of the maximum mechanical stress strength value is 401.66Mpa, and the value of the average mechanical stress strength is 67.12Mpa. Fig 25(b) shows the Von Mises stress distribution diagram of the rotor when the IPMSM running with the highest speed of 18000rpm stops suddenly with the braking acceleration 30000rad/s^2. It can be found that the maximum mechanical stress points of the IPMSM with optimized I2V rotor topology structure is also located on the junctions of rib1.The value of the maximum mechanical stress strength value is 396.43Mpa, and the value of the average mechanical stress strength is 67.12Mpa. Figure 25(c) shows the Von Mises stress distribution diagram of the rotor when the speed is 18000rpm and the rotor temperature is 130°.It can be found that the maximum mechanical stress points of the IPMSM with optimized I2V rotor topology structure is also located on the junctions of rib1, the value of the maximum mechanical stress strength value is 387.13Mpa, and the value of the average mechanical stress strength is 90.70Mpa. The values of the maximum mechanical stress of the rotor under the above three operating conditions do not exceed the maximum yield strength of the steel. Therefore, the rotor bridges and ribs will not rupture.

The results of FEA total deformation of the rotor under different working conditions are shown in Figure 26. Figure 26(a) shows the distribution diagram of the displace-ment of mechanical deformation of the rotor at the highest speed of 18000rpm. It can be found that the largest displacement point of mechanical deformation is located at the center of the bridge3, the value of the maximum displacement

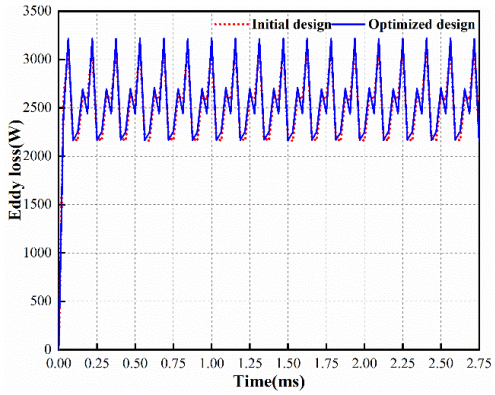

(a)The Comparison of the eddy loss

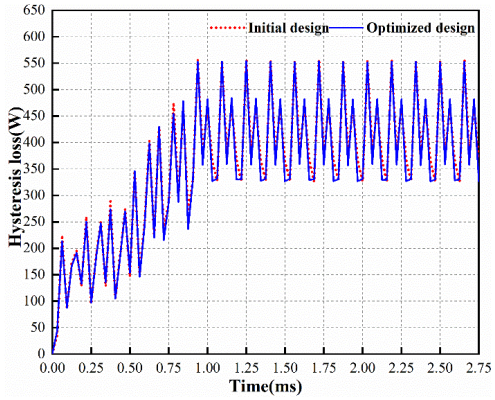

(b) The Comparison of the hysteresis loss

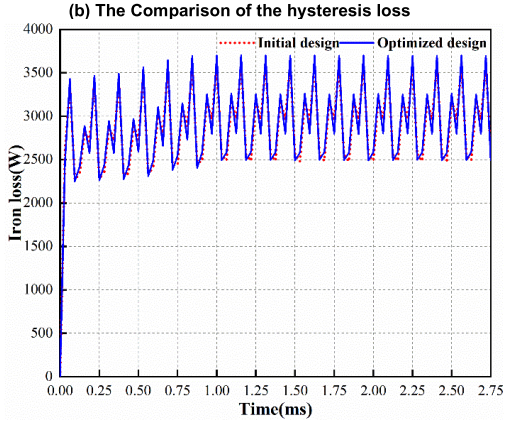

(c) The Comparison of the total iron loss

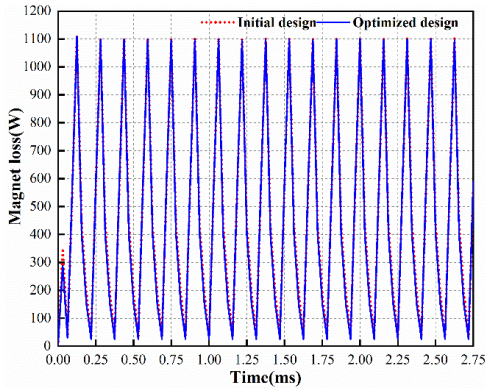

(d) The Comparison of the magnet loss

FIGURE 24. The Comparison of the iron loss of the IPMSM under deep flux weakening conditions after the further optimization.

(a)The working conditions with the speed 18000rpm

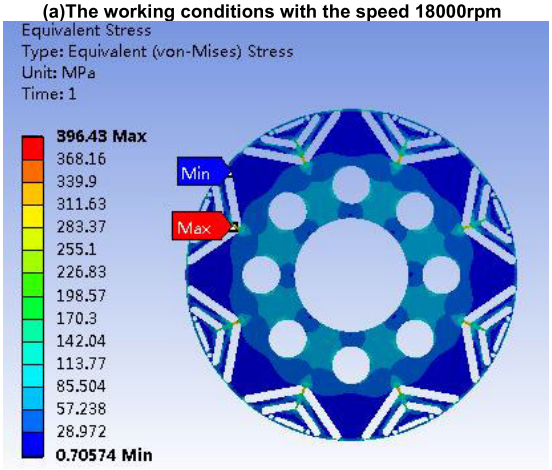

(b)The working conditions with the braking acceleration 30000rad/s2

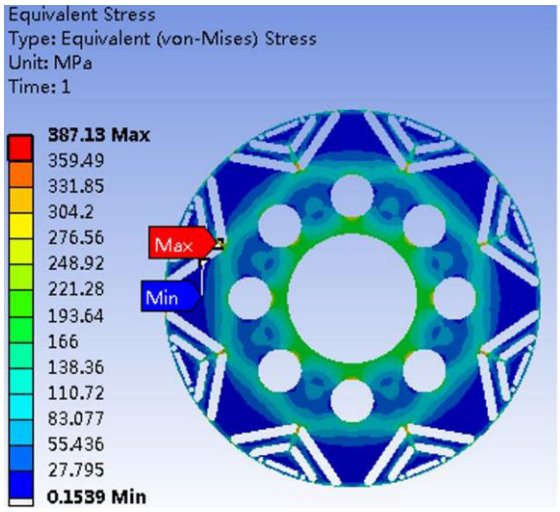

(c)The working conditions with the rotor temperature130℃

FIGURE 25. The Comparison of the FEA von Mises stress of rotor under different working conditions.

of mechanical deformation is 0.04649mm, and the value of the average displacement of mechanical deformation is 0.01688mm. Figure 26(b) shows the distribu- tion diagram of mechanical the displacement of mechanical deformation of the rotor when the IPMSM running at the highest speed of 18000rpm stops suddenly with the braking

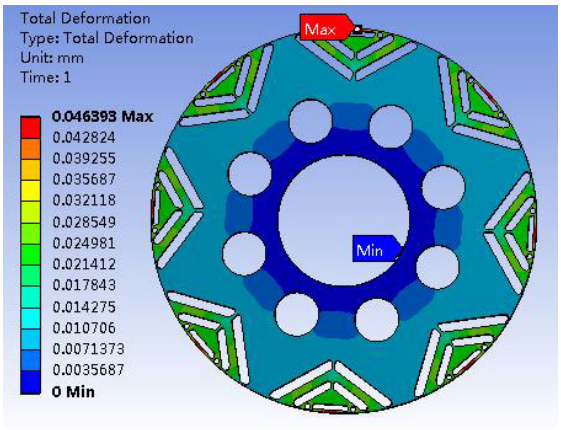

(a)The working conditions with the speed 18000rpm

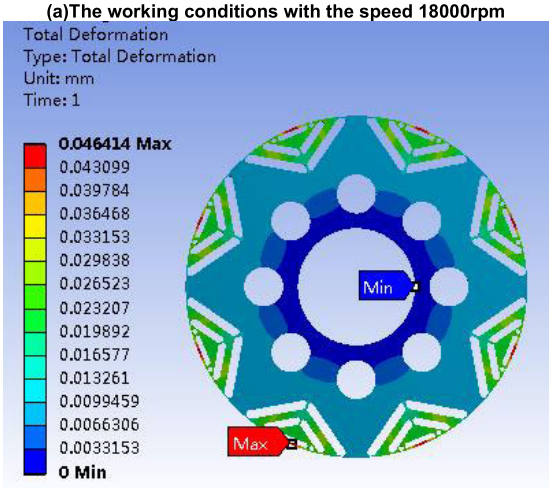

(b)The working conditions with the braking acceleration 30000rad/s2

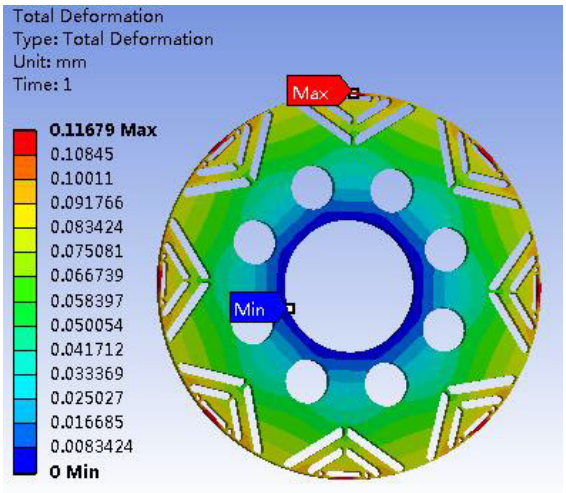

(c)The working conditions with the rotor temperature130℃

FIGURE 26. The Comparison of the FEA total displacement of rotor deformation under different working conditions.

acceleration 30000 rad/s^2. It can be found that the largest displacement point of mechanical deformation is located at the center of the bridge3, the value of the maximum displacement of mechanical deformation is 0.04641mm, and the value of the average displacement of mechanical deformation is 0.01692mm. Figure 26(c) shows the distribu- tion diagram of the displacement of mechanical deform-ation of the rotor when the speed is 18000rpm and the rotor temperature is 130°C. It can be found that the largest displacement point of mechanical deformation is located at the center of the bridge3, the value of the maximum displacement of mechanical deformation is 0.11679mm, and the value of the average displacement of mechanical deformation is 0.07174mm. In the above operating conditi-ons, when the rotor temperature is 130°C, the displacement value of mechanical deformation of the rotor is the largest, However, the displacement value of mechanical deforma-tion is far less than the length of the air gap, so the result in touch between stator and rotor will not occur.

V. CONCLUSION

1) The eddy loss, hysteresis loss and total iron loss of the IPMSM with three optimized rotor topology structures under different working conditions are analyzed and compared. The results show that the iron loss of the IPMSM with I2V type rotor topology structure proposed in this paper is the lowest, especially in the high speed and deep flux weakening condition. The iron loss of the IPMSM with I2V type rotor topology structure proposed in this paper is significantly less than that of the other two rotor topology structures, which improves the operation range of high efficiency area.

2) The output average torque of the IPMSM with three different rotor topology structures versus different current angles, current densities and speeds are compared and analyzed. The results show that torque performance of the IPMSM with I2V type rotor topology structure proposed in this paper are better than that of the other two rotor topologies under different working conditions. The methods of optimizing torque ripple proposed in papers [23], [24], [25], [26] are all relatively complex and costly, however the output average torque decreases greatly while reducing torque ripple and these methods can only reduce torque ripple. This paper proposes a simple and effective method to add a set of circular flux isolation holes between the second layer and the third layer of permanent magnets, and the position and diameter of this set of circular flux isolation holes are optimized and adjusted by establishing a parameterized model of circular magnetic isolation holes. The further optimized results show that the torque ripple and cogging torque of the IPMSM with I2V type rotor topology structure proposed in this paper are greatly reduced and at the same time the iron loss and the magnet loss are also further reduced, which can further improve the operating range of the high efficiency area of the motor and reduce the risk of irreversible demagnetization of the permanent magnet.

3)The von Mises stress and the total displacement of mechanical deformation of the rotor of the IPMSM with optimized I2V type under different working conditions are verified by FEA. The results show that the optimized I2V type rotor structure of the IPMSM will not rupture under different

working conditions. The displacement of the rotor deformation under different working conditions is small enough to avoid the phenomenon of the touch between stator and rotor caused by excessive displacement.

4) As the total volumes of permanent magnet of the three rotors are almost the same, the more pieces of magnet are divided, the greater the magnet loss is, making the magnet loss of the IPMSM with I2V type rotor topology structure proposed in this paper the highest in three rotors.

The I2V type rotor topology should be further optimized to effectively reduce the magnet loss in the future research.

REFERENCES

[1] T. Wenming and J. Ming, "A quasi-3-D analytical model of magnetic field for axial-flux motor based on conformal mapping method considering end effect," *Electr. Mach. Control*, vol. 25, no. 8, p. 47, 2021.

[2] P. Gao et al., "Optimization design of PCB distributed winding for axial flux permanent magnet wind generator," *Electr. Mach. Control*, vol. 25, no. 4, p. 32, 2021.

[3] W. Boxi, W. Zhenping, and Z. Kun, "Design of reentrant cooling channel in permanent magnet synchronous motor considering temperature field and flow field," *Trans. China Electrotech. Soc.*, vol. 34, no. 11, p. 2306, 2019.

[4] S.-B. Jun, J.-S. Kim, B. Son, Y.-J. Kim, S. Seo, and S.-Y. Jung, "Study on the method for reducing AC copper loss of interior permanent magnet synchronous motor," in *Proc. 21st Int. Conf. Electr. Mach. Syst. (ICEMS)*, Jeju, South Korea, Oct. 2018, p. 289.

[5] Y. Shenbo, J. Shuang, and X. Pengpeng, "Analysis and calculation for air gap open circuit air gap leakage and circuit air gap flux density of disc motor," *Electr. Mach. Conttol*, vol. 25, no. 7, p. 61, 2021.

[6] X. Sun, C. Hu, J. Zhu, S. Wang, W. Zhou, Z. Yang, G. Lei, K. Li, B. Zhu, and Y. Guo, "MPTC for PMSMs of EVs with multi-motor driven system considering optimal energy allocation," *IEEE Trans. Magn.*, vol. 55, no. 7, pp. 1–6, Jul. 2019.

[7] Y. Yang, S. M. Castano, R. Yang, M. Kasprzak, B. Bilgin, A. Sathyan, H. Dadkhah, and A. Emadi, "Design and comparison of interior permanent magnet motor topologies for traction applications," *IEEE Trans. Transport. Electrific.*, vol. 3, no. 1, pp. 86–97, Oct. 2016.

[8] F. Momen, K. Rahman, and Y. Son, "Electrical propulsion system design of Chevrolet Bolt battery electric vehicle," *IEEE Trans. Ind. Appl.*, vol. 55, no. 1, pp. 376–384, Jan./Feb. 2019.

[9] Y. Shen and Z. Q. Zhu, "Analytical prediction of optimal split ratio for fractional-slot external rotor PM brushless machines," *IEEE Trans. Magn.*, vol. 47, no. 10, pp. 4187–4190, Oct. 2011.

[10] M. Barcaro, N. Bianchi, and F. Magnussen, "Rotor flux-barrier geometry design to reduce stator iron losses in synchronous IPM motors under FW operations," *IEEE Trans. Ind. Appl.*, vol. 46, no. 5, pp. 1950–1958, Sep. 2010.

[11] F. Parasiliti, M. Villani, S. Lucidi, and F. Rinaldi, "Finite-element-based multiobjective design optimization procedure of interior permanent magnet synchronous motors for wide constant-power region operation," *IEEE Trans. Ind. Electron.*, vol. 59, no. 6, pp. 2503–2514, Jun. 2012.

[12] F. Chai, P. Liang, Y. Pei, and S. Cheng, "Analytical method for iron losses reduction in interior permanent magnet synchronous motor," *IEEE Trans. Magn.*, vol. 51, no. 11, pp. 1–4, Nov. 2015.

[13] K. Yamazaki, M. Kumagai, T. Ikemi, and S. Ohki, "A novel rotor design of interior permanent-magnet synchronous motors to cope with both maximum torque and iron-loss reduction," *IEEE Trans. Ind. Appl.*, vol. 49, no. 6, pp. 2478–2486, Nov. 2013.

[14] C. Tang, W. L. Soong, T. M. Jahns, and N. Ertugrul, "Analysis of iron loss in interior PM machines with distributed windings under deep field weakening," *IEEE Trans. Ind. Appl.*, vol. 51, no. 5, pp. 3761–3772, Sep. 2015.

[15] S. H. Han, T. M. Jahns, and Z. Q. Zhu, "Design tradeoffs between stator core loss and torque ripple in IPM machines," *IEEE Trans. Ind. Appl.*, vol. 46, no. 1, pp. 187–195, Jan. 2010.

[16] G. Pellegrino, P. Guglielmi, A. Vagati, and F. Villata, "Core losses and torque ripple in IPM machines: Dedicated modeling and design tradeoff," *IEEE Trans. Ind. Appl.*, vol. 46, no. 6, pp. 2381–2391, Nov./Dec. 2010.

[17] M. Cheng and S. Zhu, "Calculation of PM eddy current loss in IPM machine under PWM VSI supply with combined 2-D FE and analytical method," *IEEE Trans. Magn.*, vol. 53, no. 1, pp. 1–12, Jan. 2017.

[18] K. Xie, D. Li, R. Qu, Z. Yu, Y. Gao, and Y. Pan, "Analysis of a flux reversal machine with quasi-Halbach magnets in stator slot opening," *IEEE Trans. Ind. Appl.*, vol. 55, no. 2, pp. 1250–1260, Mar. 2019.

[19] J. G. Zhu and V. S. Ramsden, "Improved formulations for rotational core losses in rotating electrical machines," *IEEE Trans. Magn.*, vol. 34, no. 4, pp. 2234–2242, Jul. 1998.

[20] V. Ruuskanen, J. Nerg, M. Rilla, and J. Pyrhönen, "Iron loss analysis of the permanent-magnet synchronous machine based on finite-element analysis over the electrical vehicle drive cycle," *IEEE Trans. Ind. Electron.*, vol. 63, no. 7, pp. 4129–4136, Jul. 2016.

[21] D.-K. Lim, K.-P. Yi, D.-K. Woo, H.-K. Yeo, J.-S. Ro, C.-G. Lee, and H.-K. Jung, "Analysis and design of a multi-layered and multi-segmented interior permanent magnet motor by using an analytic method," *IEEE Trans. Magn.*, vol. 50, no. 6, pp. 1–8, Jun. 2014.

[22] G. Traxler-Samek, T. Lugand, and M. Uemori, "Vibrational forces in salient pole synchronous machines considering tooth ripple effects," *IEEE Trans. Ind. Electron.*, vol. 59, no. 5, pp. 2258–2266, May 2012.

[23] Q. Ronghai and Q. Chuan, "Development status and prospects of electric vehicles and their drive motors," *Southern Power Syst. Technol.*, vol. 10, no. 3, pp. 82–86, 2016.

[24] J. A. Güemes, A. M. Iraolagoitia, J. I. Del Hoyo, and P. Fernández, "Torque analysis in permanent-magnet synchronous motors: A comparative study," *IEEE Trans. Energy Convers.*, vol. 26, no. 1, pp. 55–63, Mar. 2011.

[25] C. Shukang, H. Gong, F. Chai, and H. W. Gao, "Study on cogging torque of permanent magnet in-wheel motor," *Proc. CSEE*, vol. 29, no. 30, pp. 47–51, 2009.

[26] B. Stumberger, A. Hamler, and V. Gorican, "Accuracy of iron loss estimation in induction motors by using different iron loss models," *J. Magn. Magn. Mater.*, vol. 24, no. 7, pp. 272–276, 2003.

[27] H. Fang, R. Qu, J. Li, P. Zheng, and X. Fan, "Rotor design for high-speed high-power permanent-magnet synchronous machines," *IEEE Trans. Ind. Appl.*, vol. 53, no. 4, pp. 3411–3419, Jul. 2017.

[28] F. Zhang, G. Du, T. Wang, G. Liu, and W. Cao, "Rotor retaining sleeve design for a 1.12 MW high-speed PM machines," *IEEE Trans. Ind. Appl.*, vol. 51, no. 5, pp. 3675–3685, Apr. 2015.

LIANBO NIU was born in Henan, China, in 1980. He received the B.S. degree in electrical engineering from the Jiaozuo Institute of Technology, Jiaozuo, China, in 2003, and the M.S. degree from the School of Electrical Engineering and Automation, Henan Polytechnic University, Jiaozuo, in 2010. He is currently pursuing the Ph.D. degree with the School of Mechanical and Electronically Engineering, Henan University of Science and Technology.

His current research interests include the modeling, design, and analysis of permanent-magnet synchronous motors for traction applications.

MINGZHU ZHANG was born in Henan, China, in 1964. He received the Ph.D. degree from the Xian University of Technology, Xian, China, in 2007.

He is a Professor with the School of Mechanical and Electronically Engineering, Henan University of Science and Technology. His research interests include the vehicle transmission and control and modern digital control.